IN-47
7281
044

NASA Contractor Report 4361

Analysis of Error in TOMS Total Ozone as a Function of Orbit and Attitude Parameters

W. W. Gregg, P. E. Ardanuy, W. C. Braun,
B. J. Vallette, P. K. Bhartia, and S. N. Ray

CONTRACT NAS5-29373
APRIL 1991

(NASA-CR-4361) ANALYSIS OF ERROR IN TOMS TOTAL OZONE AS A FUNCTION OF ORBIT AND ATTITUDE PARAMETERS (Research and Data Systems) 44 p CSCL 04B
N91-21670
Unclas
H1/47 0007281

NASA Contractor Report 4361

Analysis of Error in TOMS Total Ozone as a Function of Orbit and Attitude Parameters

W. W. Gregg, P. E. Ardanuy,
W. C. Braun, and B. J. Vallette
Research and Data Systems Corporation
Greenbelt, Maryland

P. K. Bhartia
Consultant
Mitchellville, Maryland

S. N. Ray
Software Corporation of America
Bowie, Maryland

Prepared for
Goddard Space Flight Center
under Contract NAS5-29373

National Aeronautics and
Space Administration
Office of Management
Scientific and Technical
Information Division

1991

TABLE OF CONTENTS

PRECEDING PAGE BLANK NOT FILMED

PAGE ii INTENTIONALLY BLANK

ABSTRACT

Computer simulations of orbital scenarios were performed in order to examine the effects of 1) orbital altitude, 2) equator crossing time, 3) attitude uncertainty, and 4) orbital eccentricity on ozone observations by potential future satellites. These effects were assessed in two ways: 1) by determining changes in solar and viewing geometry (solar and spacecraft zenith angles, and relative azimuth angle) and/or 2) by determining Earth daytime coverage loss. The importance of changes in geometry on ozone retrieval was determined by simulating uncertainties in the TOMS ozone retrieval algorithm. The major findings, rated in order of importance, are delineated below.

1. Drift of the equator crossing time (ECT) from local noon would have the largest effect on the quality of ozone derived from TOMS. The most significant effect of this drift is the loss of Earth daytime coverage in the winter hemisphere. The loss in coverage increases nonlinearly with the drift in local time, from 1° latitude for ± 1 hour from noon, 6° in latitude for ± 3 hours from noon, to 53° for ± 6 hours from noon. Maximum daytime coverage occurred for the local noon ECT. An additional effect is the increase in ozone retrieval errors due to high average solar zenith angles.

2. To maintain contiguous Earth coverage, the maximum scan angle of the sensor must be increased with decreasing orbital altitude. The maximum scan angle required for full coverage at the equator varies from 60° at 600 km altitude to 45° at 1200 km. The increase in scan angle produces an increase in spacecraft zenith angle θ, which decreases the ozone retrieval accuracy. The range in θ was $\approx 72°$ for 600 km to $\approx 57°$ at 1200 km. However, because of scan overlap between adjacent orbits the highest spacecraft zenith angles are required only at the equator. Despite overlap there is a unique scan angle required to view the poles for each altitude. The θ associated with these scan angles ranged from 62.5° at 600 km to 52° at 1200 km.

3. The effect of elliptical orbits is to create gaps in coverage along the subsatellite track. An elliptical orbit with a 200 km perigee and 1200 km apogee produced a maximum Earth coverage gap of about 45 km at the perigee at nadir (this equals about 1 Nimbus-7 TOMS pixel on the ground). The gap travels on the Earth from the pole to the equator in a month. Orbits with less eccentricity produce smaller coverage gaps.

4. An attitude uncertainty of 0.1° in each axis (pitch, roll, yaw) produced a maximum ozone retrieval error of 1.3 Dobson Units (DU) at 955 km under the worst conditions (maximum attitude configuration, maximum scan angle to view the pole, and maximum solar zenith angle). The error decreased for lower altitudes and increased for higher altitudes, reaching a maximum of 1.4 DU at 1200 km.

1.0 INTRODUCTION

After 11 years of continuous operation, the Total Ozone Mapping Spectrometer (TOMS) on Nimbus-7 is nearing the end of its useful life. For the purpose of providing continuous coverage and assessing the long-term trends of atmospheric ozone, it is essential that a follow-on sensor be flown. To maximize the acquisition of a long-term data base, the follow-on TOMS would preferably be flown in a Nimbus-7-type orbit. However, the availability of funds and launch vehicles may dictate that the sensor be flown in a different orbital configuration. It is important to know the impacts of these orbital and sensor parameters on ozone retrieval before launch in order to determine the limits of acceptability of the orbital configurations. The purpose of this study is to examine the importance of orbital and attitude parameters on the retrieval of ozone, by emphasizing the effects on solar and viewing geometry. Nimbus-7 TOMS results have shown that errors in ozone retrieval are functions of the solar zenith angle, spacecraft zenith angle, and total ozone. The solar and spacecraft zenith angles are directly related to the selection of orbit. Azimuthal dependence was unimportant for Nimbus-7 (nearly constant for the ascending node) but may become important for other orbits. Thus the study focuses on assessing the variation of solar and spacecraft geometry as a function of orbital altitude and equator crossing time (ECT), and secondarily their potential effect on ozone retrievals using the TOMS ozone retrieval algorithm. The study also assesses the changes in Earth daytime coverage due to changing ECT and elliptical orbits. Hopefully, this study provides useful information from which launch decisions may be made.

1.1 Nimbus-7 and TOMS

Nimbus-7, which contained seven other sensors in addition to TOMS, was launched in 1978 into a Sun-synchronous, noon local ECT, near-circular orbit at 955 km. Relevant platform characteristics of Nimbus-7 and sensor characteristics of TOMS are summarized in Table 1. After 11 years the Nimbus-7 orbital parameters have changed only slightly, as shown in Table 2. The ECT has varied from ± 45 min. of noon.

The follow-on TOMS is proposed to fly on the SCOUT vehicle. The orbital parameters for SCOUT have not yet been decided, but the TOMS sensor will be similar to the Nimbus-7 TOMS, with a 3° instantaneous field-of-view (IFOV) and scanning in steps of 3°.

2.0 METHODS

2.1 Circular Orbit Scenarios

To examine the effect of orbital altitude on ozone retrievals, a set of 8 orbital altitudes were specified, ranging from 600 km to 1200 km in increments of 100 km, and including a 955-km orbit to simulate Nimbus-7. These orbits were selected to span the range of possible orbital altitudes for candidate launch vehicles. In this analysis, all orbits were circular (eccentricity = 0), as was Nimbus-7 (nearly).

Table 1. Nimbus-7 Orbital Parameters and TOMS Sensor Characteristics	
Nimbus-7 Orbital Parameters	
Altitude	955 km
Period	104 min
Inclination	99.3°
Equator Crossing Time	Noon Local
Eccentricity	≈0
TOMS Sensor Characteristics	
Maximum Scan Angle	51°
Scan Period	8 sec
IFOV	3°
Ground IFOV at Nadir	50 km
Pixels Along Scan	35
Ground Coverage	2,800 km

Table 2. Present Nimbus-7 Orbital Parameters	
Epoch	19900503
Semimajor Axis	7327.2 km
Eccentricity	0.0008758
Inclination	99.2°
Period	104.0 min
Perigee Height	942.6 km
Apogee Height	955.4 km

Computations of orbital and sensor characteristics of these different altitudes were subject to the following constraints:

a. The orbits were assumed Sun-synchronous with a near-noon ECT

b. The sensor scan angle was adjusted in increments of 3° to produce contiguous global coverage at the equator

c. The instantaneous field of view (IFOV) and scan step angles were kept constant at 3°.

These constraints produced orbital and sensor parameters as given in Table 3. The following describes how these parameters were computed. The inclination required to keep the orbits Sun-synchronous was computed by

$$\cos(i) = -\frac{2\Omega R_s^{3.5}}{3J_2(GM_e)^{1/2}R_e^2} \quad (1)$$

(Stewart, 1985), where i is the inclination of the subsatellite track relative to the equator, Ω is Earth's rotation rate about the Sun, R_e is the radius of the Earth, R_s is the height of the satellite measured from the center of the Earth ($= R_e + H_s$, where H_s is the altitude of the satellite above the Earth's surface), J_2 is the Earth oblateness factor, G is the universal gravitational constant, and M_e is the mass of the Earth. Values for these parameters were taken from Stewart (1985). Orbital period was computed by

$$P = 2\pi\left[\frac{R_s^3}{GM_e}\right]^{1/2} \div 60 \quad (2)$$

(Maul, 1985). Division by 60 converts period into minutes.

Table 3. Orbital and Sensor Parameters for Satellites at 8 Different Orbital Altitudes (Nimbus-7/TOMS parameters are shown for comparison)

	Altitude (km)							
	600	700	800	900	955	1000	1100	1200
Period (min)	96.54	98.63	100.73	102.74	104.01	104.97	107.11	109.27
Inclination (°)	97.78	98.18	98.60	99.03	99.27	99.47	99.93	100.41
Maximum Scan Angle (°)	60.0	57.0	54.0	51.0	51.0	49.5	48.0	45.0
Scan Period (sec)	4.5	5.4	6.3	7.3	7.8	8.2	9.2	10.3
Pixels/Scan	41	39	37	35	35	34	33	31
Ground IFOV Nadir (km)	31.4	36.7	41.9	47.1	50.0	52.4	57.6	62.9
Ground IFOV Scan Edge (Relative to Nadir)	17.5	12.8	9.9	8.0	7.3	6.8	5.8	5.2

Computation of the half scan angle required to produce contiguous Earth coverage at the equator is more complicated and requires an accompanying figure for explanation. Figure 1 shows the Earth-satellite geometry and the definition of terms used in the derivation.

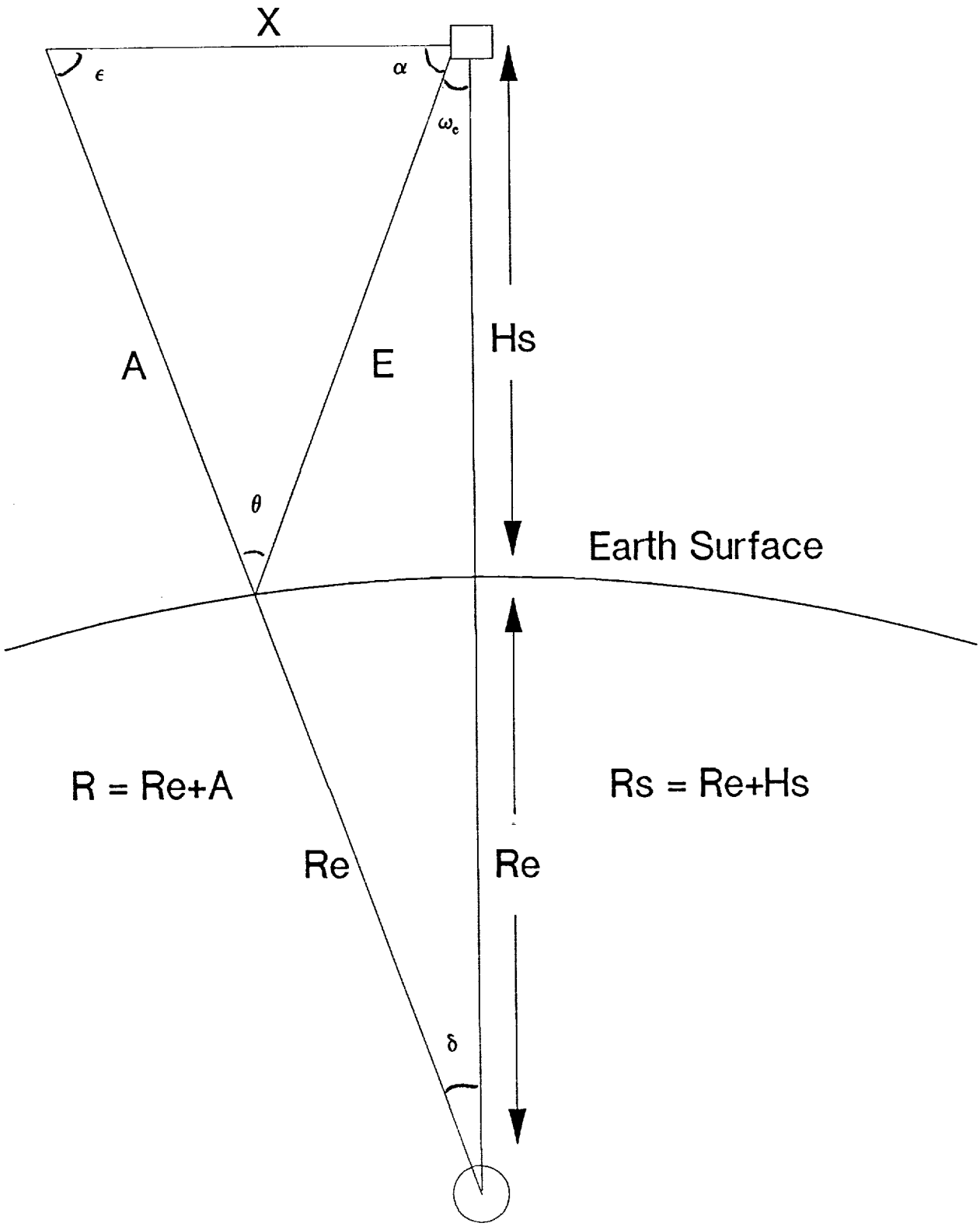

Figure 1. Schematic of Earth-satellite geometry showing terms used in computations of orbital parameters.

The problem is to find the maximum satellite scan angle ω_e, given the spacecraft altitude radius R_s and the Earth angle in degrees δ required to produce contiguous coverage at the equator from one orbit to the next. This Earth angle is determined by

$$L_2 - L_1 - 0.25(°/\text{min})P \tag{3}$$

$$\delta = |L_2|/2 \tag{4}$$

where L_1 is the longitude where the subsatellite ground track crosses the equator for the first orbit, and L_2 is the longitude of the second orbit. The satellite must scan one-half this longitudinal distance to maintain contiguous coverage, hence Eqn. 4. Inclination increases the distance the satellite must scan, and thus the Earth angle. To account for inclination, Eqn. 4 must be multiplied by 1/cos(90-i), or 1/sin(i).

The angle ϵ and the distances X and R are easily found by

$$\epsilon = 90 - \delta \tag{5}$$

$$X = R_s \tan\delta \tag{6}$$

$$R = (X^2 + Y^2)^{1/2} \tag{7}$$

To find α requires that the lengths A and E be known. This is accomplished by

$$A = R - R_e \tag{8}$$

and

$$E = [X^2 + A^2 - 2XA\cos\epsilon]^{1/2} \tag{9}$$

Using the sine rule, then

$$\sin\alpha = A/E\sin\epsilon \tag{10}$$

and clearly, $\omega_e = 90 - \alpha$.

Since this computation of the scan angle is exact (hence the subscript) and in actuality the sensor views the Earth in discrete pixels, each with a 3° field of view, it is necessary to find the scan angle actually observed by the sensor in these IFOV increments. This was accomplished by

$$N-2/3\omega_e+0.5 \quad (11)$$

$$\omega-3/2N \quad (12)$$

where N is the number of pixels in a scan. This value was then checked by computing the increase in ground IFOV at the scan edges to ensure that the pixels only slightly overlapped at the scan edge in successive orbits. This procedure resulted in minor changes in N, δ, and the maximum half-scan angle, the final values of which are shown in Table 3.

Incidentally, the angle θ in Figure 1 is defined as the spacecraft zenith angle (the angle from local zenith to the spacecraft as viewed from the ground) and is computed by

$$\sin\theta-R_s/R_e\sin\omega \quad (13)$$

This value is used to determine the path length of radiance through the atmosphere.

The scan period was computed to ensure contiguous coverage along-track at nadir considering the IFOV of 3°. As such, computation of the scan period required knowledge of the ground speed of the satellite

$$V-2\pi R_e/P \quad (14)$$

The scan period P_s to meet this requirement is then

$$P_s-IFOV*H_s/V \quad (15)$$

where IFOV is in radians and the numerator IFOV*H_s gives the ground IFOV (the instantaneous field of view on the ground in m).

2.2 Earth Location Simulation

The Earth location algorithms use the orbital data described above to find the location of a pixel on the Earth (in latitude/longitude coordinates) and the associated spacecraft and solar zenith and azimuth angles. The spacecraft zenith angle θ is defined as the angle between a vector from the pixel ground point to nadir and a vector from the pixel to the spacecraft (see Figure 1). The spacecraft azimuth angle ϕ is defined as the angle between a vector from the pixel ground location to due north and a vector from the pixel to the subsatellite ground point, measured clockwise from true north. The solar zenith θ_o and azimuth ϕ_o angles are defined analogously with respect to the Sun, and thus require, in addition to the pixel location, the time of day and day of year of the observation at the pixel location.

The Coastal Zone Color Scanner (CZCS) Geolocation Algorithms code (Wilson et al., 1981) was used to compute pixel location and spacecraft (viewing) geometry (spacecraft zenith and azimuth angles), after modification resulting from thorough investigation of the code. The code was

modified for three reasons: 1) to allow the use of different orbital and sensor parameters from those of Nimbus-7 and the CZCS, 2) to resolve quadrant ambiguities occurring primarily near the poles and the date line, and 3) to compute spacecraft azimuth relative to the pixel rather than relative to the spacecraft as computed in the code. Since this latter modification is not available in the reference, it is described here, by

$$\cos\phi = \frac{\sin\Psi_s - \cos\delta\sin\Psi_p}{\cos\Psi_s\cos\Psi_p} \tag{16}$$

where Ψ_p is the latitude of the pixel and Ψ_s is the latitude of the subsatellite ground point.

Given pixel location (latitude and longitude) by the above algorithms, time of day from the local ECT and spacecraft travel time, and day of year, the solar geometry (θ_o and ϕ_o) was computed by standard methods described in Iqbal (1983). This method includes the Equation of Time, or time correction factor, to account for asymmetry in the Earth's revolution around the Sun, such that the Sun is not directly overhead at the equator at noon at the vernal equinox.

2.3 Elliptical Orbit Scenarios

The SCOUT mission may be placed into an elliptical transfer orbit before being placed into a circular orbit. Alternatively, the orbit may deviate from a circular orbit over time. For these reasons, it is important to discuss the impact of elliptical orbits on ozone observations. A set of elliptical orbit scenarios were developed to examine this problem. Since the goal is to keep the platform as close to a Sun-synchronous one, only Sun-synchronous elliptical orbits were simulated.

For elliptical Sun-synchronous orbits, Eqn. 1 must be changed to

$$\cos(i) = \frac{2\Omega a^{3.5}(1-e^2)^2 0.9856}{3J_2(GM_e)^{1/2}R_e^2} \tag{17}$$

where a is the semimajor axis, e is the eccentricity, and other terms are as defined earlier. The eccentricity is computed by

$$e = (a - h_p - Re)/a = (h_A - h_p)/(2a) \tag{18}$$

where a is the semimajor axis, h_p is the perigee height, and h_A is the apogee height. The geometry of the problem is shown in Figure 2.

Since the expected orbit will be close to 955 km, the various Sun-synchronous elliptical orbits considered for the study were kept to configurations such that the minimum satellite altitude was 200 km or greater, and the maximum altitude, 1200 km or less. Characteristics of these orbits are presented in Table 4.

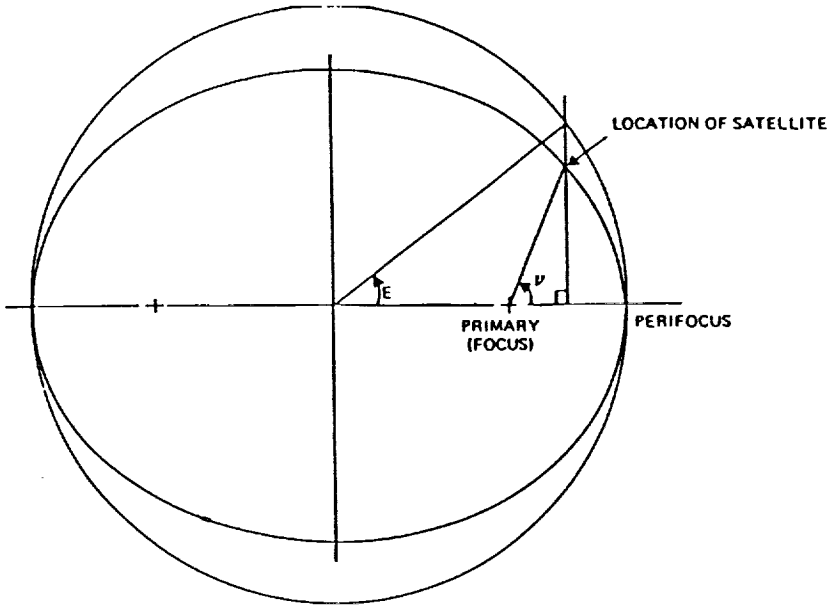

Definition of True Anomaly, ν, and Eccentric Anomaly, E. The outer figure is a circle with radius equal to the semimajor axis.

Mean Anomaly $M = E - e \sin E$

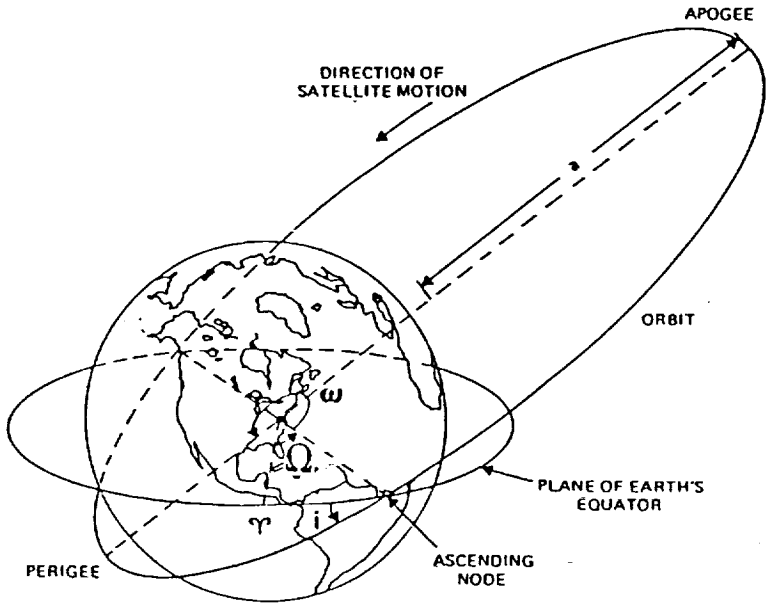

Keplerian Orbital Elements. ♈ marks the direction of the Vernal Equinox. Ω is measured in the plane of the Earth's equator, and ω is measured in the orbit plane.

Figure 2. Schematic of elements of elliptical orbits. (Reprinted from Wertz, 1978.)

Table 4. Sun-Synchronous Elliptical Orbit Scenarios					
Perigee Height (km)	Apogee Height (km)	Mean Altitude (km)	Semimajor Axis (km)	Eccentricity	Inclination (°)
400	955	677.5	7056	0.039	98.07
600	955	777.5	7156	0.025	98.50
800	955	927.5	7256	0.011	98.93
955	955	955.0	7333	0.000	99.27
200	1200	700.0	7078	0.07064	98.11

Another equation of interest is precession in the apsides, computed by

$$\Delta\zeta = -2.06474 \times 10^{14} a^{-3.5}(1-e^2)^{-2}(2-5\sin^2 i)(t-t_0) \qquad (19)$$

The elliptical orbits were generated using an orbit generation program developed by Jet Propulsion Laboratory (Khan, 1978). This FORTRAN program is adapted to run on an IBM Personal Computer. Only the J_2 component of the gravity field was considered in generating the orbit, since other terms in the potential have negligible effect.

2.4 Ozone Retrieval Algorithm

To understand the effects of solar and viewing geometry on the retrieval of ozone, it was necessary to utilize the TOMS ozone retrieval algorithm. To understand the algorithm it is helpful to review the TOMS sensor.

The TOMS sensor contains six wavelength bands (Table 5). The first two bands lie in a spectral region where ozone does not absorb, and consequently are used to determine the atmospheric reflectivity. The last four bands (the numbering is not in spectral order) are in regions where ozone absorbs, and it is these bands that are primarily used to determine ozone.

The TOMS ozone algorithm is essentially an interpolation of a precomputed table relating predicted radiance received by the sensor to ozone amount, for a series of solar and viewing geometries. The look-up table contains radiance values determined by multiple scattering theory. To account for the variation in the shape of the ozone profiles with latitude and with total ozone, the current algorithm (Version 6) uses three sets of profiles: a set of three profiles for 15°S to 15°N, a set of ten profiles for the 45° latitude, and another set of ten profiles for all latitudes poleward of 75°. In the current implementation, the profiles are assumed hemispherically symmetrical. Between 15° and 75°, the ozone amounts are independently derived from the adjacent set of profiles and linearly interpolated to the measurement latitude.

Table 5. Bands of the TOMS Sensor and Associated Ozone Absorption Coefficients

Wavelengths are in Angstroms and absorption coefficients in $(atm\text{-}cm)^{-1}$

Band	Wavelength	Absorption Coefficient
1	3600	0
2	3800	0
3	3125.14	1.64870
4	3175.12	0.87349
5	3312.53	0.14054
6	3398.61	0.02450

Given solar viewing geometry, latitude, and an ozone profile, the algorithm produces theoretical N values, where

$N = -100\log_{10}(I_o/F)$, I_o is the predicted radiance at the satellite, and F is the solar irradiance incident at the top of the atmosphere (wavelength dependence is suppressed). From the N values are derived the N-pairs, the difference of the N values at the ozone-absorbing wavelengths. There are three N-pairs, Band 3-5 (N_a, or the A pair), Band 4-6 (N_b, or the B pair), and Band 5-6 (N_c, or the C pair). Given these N-pairs and the total ozone, a relationship is constructed, known as the N tables. Examples are shown in Figure 3 for the three latitudinal bands. (The extreme solar and viewing geometries used here (Table 6) were deliberately selected to represent situations where the ozone retrieval errors would be maximum).

Given a radiance observation by the sensor, the radiances are converted into N values and eventually N-pairs for the given location and geometry. Three independent estimates of total ozone are obtained using the pairs defined earlier. These three independent estimates combined into a weighted mean, called the "best ozone" by the algorithm. Individual pair weights W_i are calculated as follows.

$$W_i = \left[\frac{(dN/d\Omega_i)^2}{\Delta\lambda_i \Delta\alpha_i}\right]^2 \tag{20}$$

where Ω is the ozone amount, the subscript i refers to the pair (A, B, or C), and the Δ, to a subtraction involving the two bands that make up the pair. Before applying these weights, they are normalized

$$W_i' = W_i/(W_A + W_B + W_C) \tag{21}$$

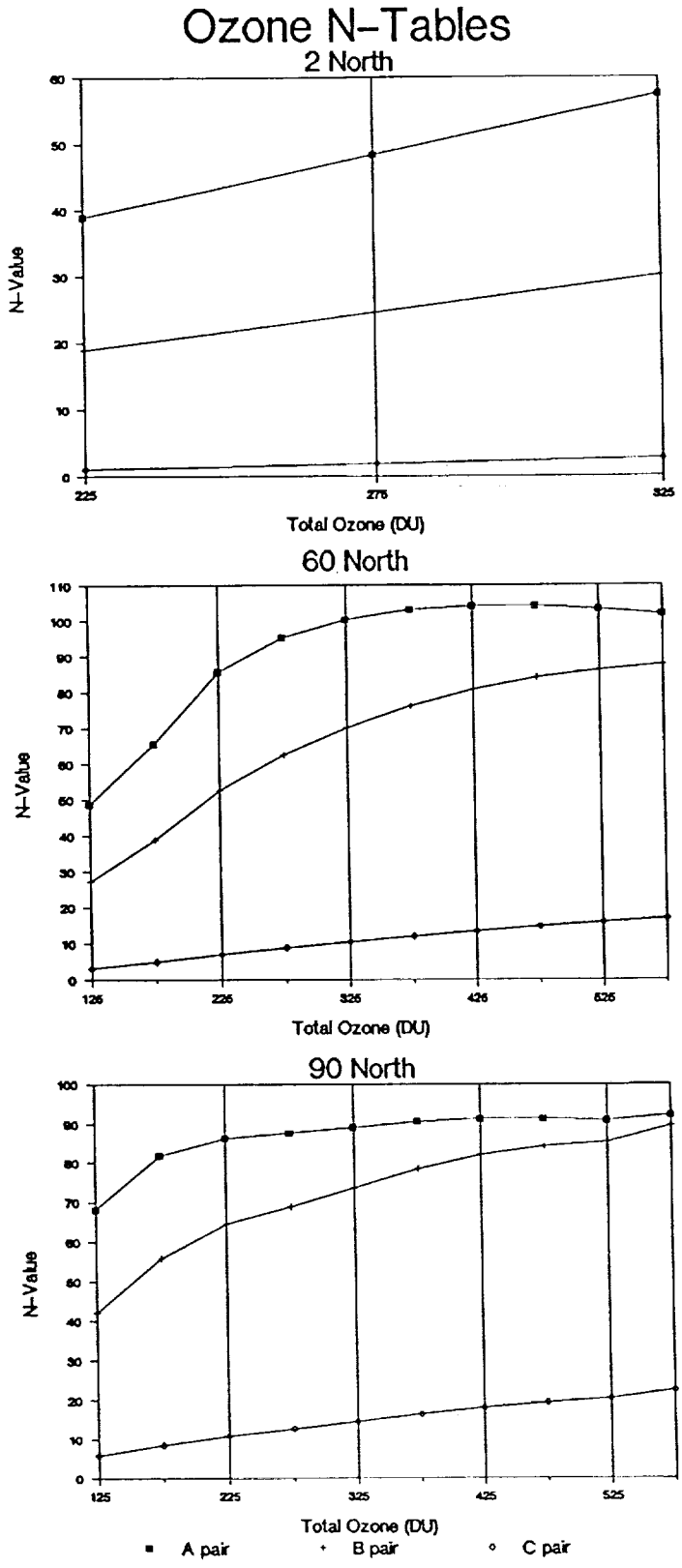

Figure 3. Ozone N-tables relating N-pairs to ozone for three latitudes. Solar and viewing geometries are in Table 6.

Table 6. Solar and Viewing Geometries for Three Latitudes Used to Obtain the Ozone N-Tables Shown in Figure 3 and Used in Later Analyses			
	2°N	60°N	90°N
θ_o	10.6°	83.6°	87.8°
θ	63.3°	38.8°	54.4°
ϕ-ϕ_o	13.1°	85.3°	-271.5°

Then

$$\Omega_{BEST} = W'_A F_A \Omega_A + W'_B F_B \Omega_B W'_C F_C \Omega_C \quad (22)$$

where the Ω_i's are the ozone estimates for each pair, and the f_i's are correction factors needed to correct for calibration-related biases between the pairs, specific for the Nimbus-7 TOMS. These factors were set to unity in the present analysis.

2.5 Ozone Retrieval Error Due to Attitude Uncertainty

The procedure for investigating ozone errors due to attitude uncertainties is described in detail in Table 7. For this effort, the maximum error in ozone due to attitude uncertainty was preferred. The viewing geometry of the North Pole was selected as the maximum scan angle with the maximum range in θ_o. This corresponded to the right-hand side of the scan. Then the attitude configuration that produced the greatest change in solar and viewing geometries for this scan position was determined, given a 0.1° maximum in each of the three axes. The configuration that produced maximum changes was:

pitch	=	0.1° (forward along subsatellite track),
roll	=	0.1° (toward the east),
yaw	=	-0.1° (toward the west).

Three initial ozone values (130, 320, and 570 DU) were used that represent low, medium, and high ozone, and are located between tabulated values in the ozone N-tables to include interpolation error. Finally, an entire year of subsolar positions was simulated to determine when the maximum error in ozone occurred. The maxima for all ozone values were in late autumn when θ_o was near maximum (> 88°); on Julian Day 261 for low ozone, Julian Day 260 for medium ozone, and Julian Day 255 for high ozone.

2.6 Ozone Retrieval Error due to Ozone Profile Uncertainty

In the current TOMS algorithm, perhaps the most serious error in deriving total ozone is the error due to profile shape uncertainty (Stolarski et al., 1990). As described by Klenk et al., (1982), this error increases with increasing optical path length, and is hence a function of θ_o, θ, and the total ozone amount.

Table 7. Determination of Error Due to Attitude Uncertainty	
1.	Select Geometry θ_o, θ, ϕ-ϕ_o a. For 90°N. b. Three ozone amounts, low (130 DU), medium (320 DU), high (570 DU).
2.	Compute upper- and lower-bound ozone for each ozone amount (e.g., for 320 DU, lower-bound is 275 DU, upper-bound is 325 DU, since the ozone N-Tables are in increments of 50 DU).
3.	Compute N-values and N-pairs at upper- and lower-bounds for each zone amount. These are the N-tables to be used for computation of ozone.
4.	Change geometry to +0.1° pitch, +0.1° roll, -0.1° yaw.
5.	Compute N-values and N-pairs for this new geometry.
6.	Use the N-table computed in Step 3 to compute ozone for each N-pair using linear interpolation.
7.	Weigh the ozone values in Step 6 to obtain "Best Ozone."
8.	Subtract input ozone from ozone computed in Step 7 = ϵ (error).
9.	Perform for each altitude.

Table 8. Determination of Error Due to Ozone Profile Uncertainty	
1.	Select Geometry θ_o, θ, ϕ-ϕ_o a. For three latitudes (2°N, 60°N, 90°N). b. Three ozone amounts, low (130 DU), medium (320 DU), high (570 DU).
2.	Compute upper- and lower-bound ozone for each ozone amount (e.g., for 320 DU, lower-bound is 275 DU, upper-bound is 325 DU, since the ozone N-Tables are in increments of 50 DU).
3.	Compute N-values and N-pairs at upper- and lower-bounds for each zone amount. These are the N-tables to be used for computation of ozone.
4.	Change latitude, keeping geometry fixed to next highest latitude bin for low and mid-latitudes; next lowest latitude bin for high latitude.
5.	Compute N-values and N-pairs at this new latitude.
6.	Use the N-table computed in Step 3 to compute ozone for each N-pair using linear interpolation.
7.	Weigh the ozone values in Step 6 to obtain "Best Ozone."
8.	Subtract input ozone from ozone computed in Step 7 = ϵ (error).

To simulate the effect of this uncertainty, the procedure outlined in Table 8 was used. The key feature of this procedure is to use the difference in total ozone amount derived from the two sets of standard ozone profiles, for latitudes closest to the measurement latitude, as a measure of profile uncertainty. Although the error for any single retrieval cannot be predicted without knowledge of the exact ozone profile, it is expected that the errors derived using our procedure provide a rough measure of the profile sensitivity of the TOMS ozone algorithm. A more complete treatment of this problem is beyond the scope of this study.

Nevertheless, this profile uncertainty is taken here to be a measure of the inherent error of the TOMS ozone algorithm, in order to quantify the effects of changing solar and viewing geometry and ECT on ozone retrieval. It is not as complete as the inherent error of the algorithm, but suffices here to show a measure of the dependence of the algorithm on the variables under consideration here.

This procedure (Table 8) is analogous to the method for determining attitude uncertainty. In this case, however, the effects of this profile uncertainty were simulated as a function of altitude and ECT. Again three ozone amounts were selected: low (130 DU), medium (320 DU), and high (570 DU). Each was used to create the N-tables at solar and viewing geometry for each altitude and ECT, but this time for each of three latitudes; equator, mid-latitude, and polar.

Unlike the determination of error due to attitude perturbations, here three locations were selected to examine the errors due to profile uncertainty: equator (2°N), mid-latitude (60°N), and the pole. For each latitude, the scan angle was determined as the maximum required to produce full Earth coverage with successive orbit scan overlap accounted for. Since there is no overlap at the equator, the maximum scan angle was used. Also, as discussed before, a unique viewing geometry is required for each orbit to view the pole. At mid-latitude, scan overlap must be accounted for. The maximum spacecraft zenith angles with no overlap at this latitude are shown in Table 9.

Table 9. Maximum Zenith Angle at Mid-Latitude ≈60°N to Produce Full Earth Coverage Considering Scan Overlap by Successive (Preceding) Orbits

Altitude (km)	600	700	800	900	955	1000	1100	1200
Max. θ	50.7	44.3	41.4	38.4	38.8	37.2	35.9	36.5

The lack of smoothness in these θ's is due to the peculiarities of orbital coverage, period, altitude, and discrete pixel packaging. Overlap regions were selected directly from plots of Earth coverage by the different altitudes.

Also, instead of selecting a day for which errors were maximum, as in the case of the attitude sensitivity analyses, the error was computed as RMS throughout the year. This takes into account the changing solar zenith angles through the year.

3.0 RESULTS AND DISCUSSION

3.1 Solar and Viewing Geometry Dependence on Altitude for Circular Orbits

For the circular orbit scenarios, Earth location simulation code allowed the determination of the effects of orbital altitude on the solar and viewing geometries (specifically, solar and spacecraft zenith angles, and relative azimuth). This part of the analyses focuses on the changes in solar and viewing geometry as a function of altitude for these circular orbits.

One of the largest differences in the circular orbit scenarios was the maximum scan angle required to maintain full coverage. It ranged from 60° for the 600-km orbit to 45° for the 1200-km orbit (Table 3). These scan angles directly affect the spacecraft zenith angle for the orbits through Eqn. 13. The maximum spacecraft zenith angles produced by these orbital altitudes are depicted in Figure 4. The zenith angles range from $\approx 72°$ for 600 km to $\approx 57°$ at 1200 km.

The effect of these changes in scan angles, however, is not as serious as one might think. Because of scan overlap at higher latitudes, these maximum θ's are required for ozone observations only at the equator.

However, there is a unique spacecraft geometry for each orbit required to view the poles. Since at the poles the solar zenith angle ozone attains maximum for near-noon ECT's, changes in θ to view the poles as a function of altitude may be an important factor in ozone retrievals. These angles are shown in Figure 5. The range in θ is from $\approx 62°$ to 51.5° (Figure 5). The patterns shift discontinuously because these data were generated by selecting the pixel nearest the North Pole for each orbit; the sensor scan steps are discrete. An analytical solution for θ as a function of altitude would yield a monotonic distribution, but the numerical solution used here is more realistic, conveying some of the peculiarities of satellite observations.

The effect of altitude on solar zenith angle is shown in Figure 6 as a histogram of the frequency of occurrence of θ_o in bins as a function of altitude. All computations were for a noon ECT at the equinox. Changing the day of year had no effect on the results. Frequency of occurrence is shown in order to minimize the effect of the different number of pixels required to maintain contiguous Earth coverage as a function of altitude. In contrast to θ, there is no effect of altitude on θ_o (Figure 6), as long as the orbits are Sun-synchronous and at the same ECT. This has major repercussions on the selection of orbit, since θ_o is a major contributor to the error in ozone retrievals. The analyses presented here demonstrate that orbital altitude will not affect the retrieval of ozone, at least as related to θ_o, if a Sun-synchronous orbit and an optimal ECT are maintained. Analysis of the effect of different ECTs will be discussed shortly.

There were relatively minor differences in relative azimuth angle (ϕ-ϕ_o) as a function of altitude (Figure 6). The small differences that did occur were the result of ϕ, rather than θ_o, and were actually the result of pixel discretization. It is reasonable to conclude that, like θ_o, orbital altitude has negligible effect on ozone retrieval, as long as the orbit is Sun-synchronous and near-noon.

3.2 Effects of ECT on Solar Geometry

The ECT is the local time at which the subsatellite track crosses the equator on ascending node. For Sun-synchronous orbits, this local time is the same for every orbit. Though the local times vary along orbit, it remains constant for any given point. For example, for a noon ECT, the satellite will cross the South Pole in the afternoon or evening and the North Pole in the morning. But the local time at which the satellite crosses the North or South Pole will be the same for every orbit.

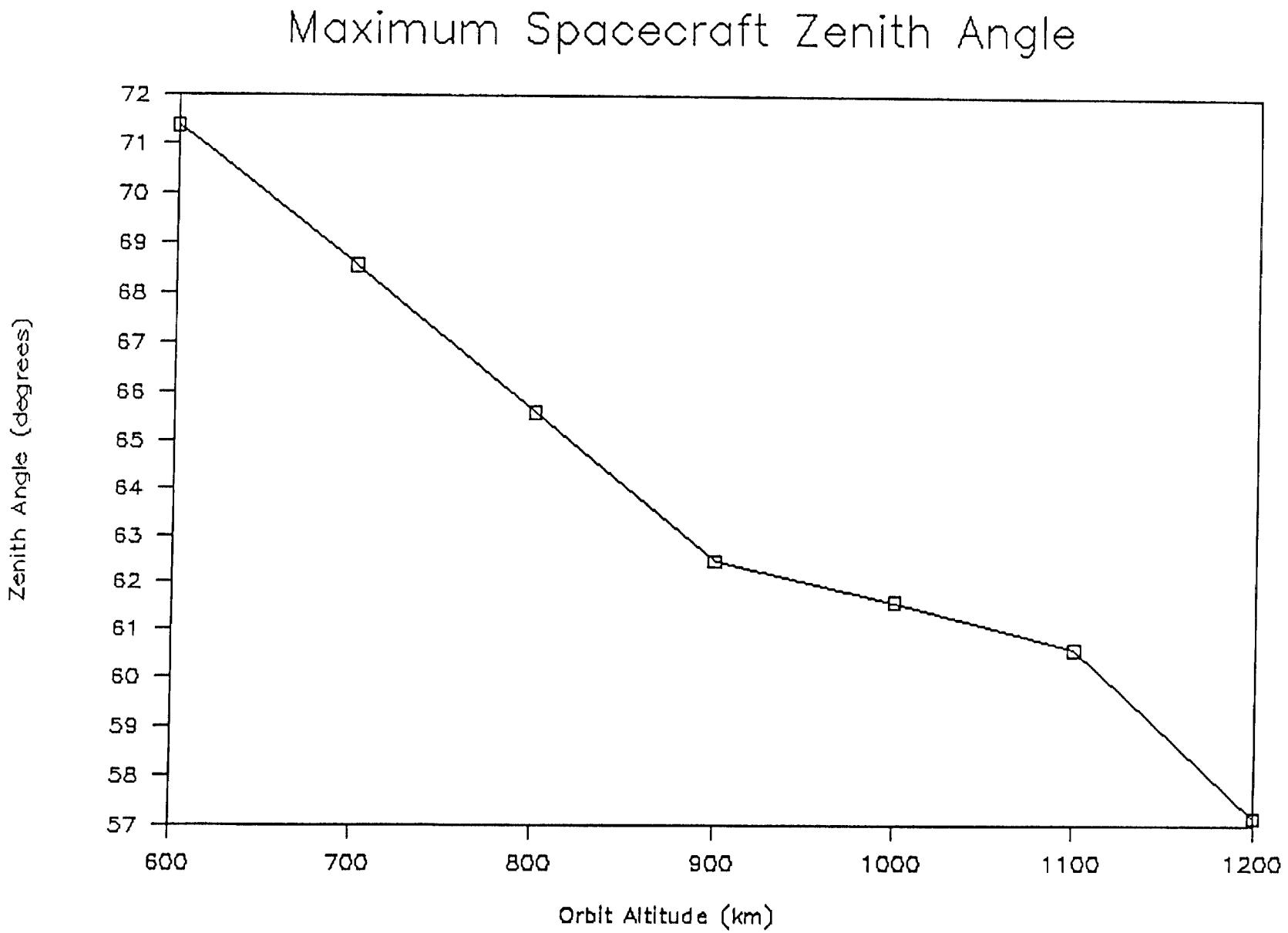

Figure 4. Maximum spacecraft zenith angle θ required for contiguous Earth coverage at the equator.

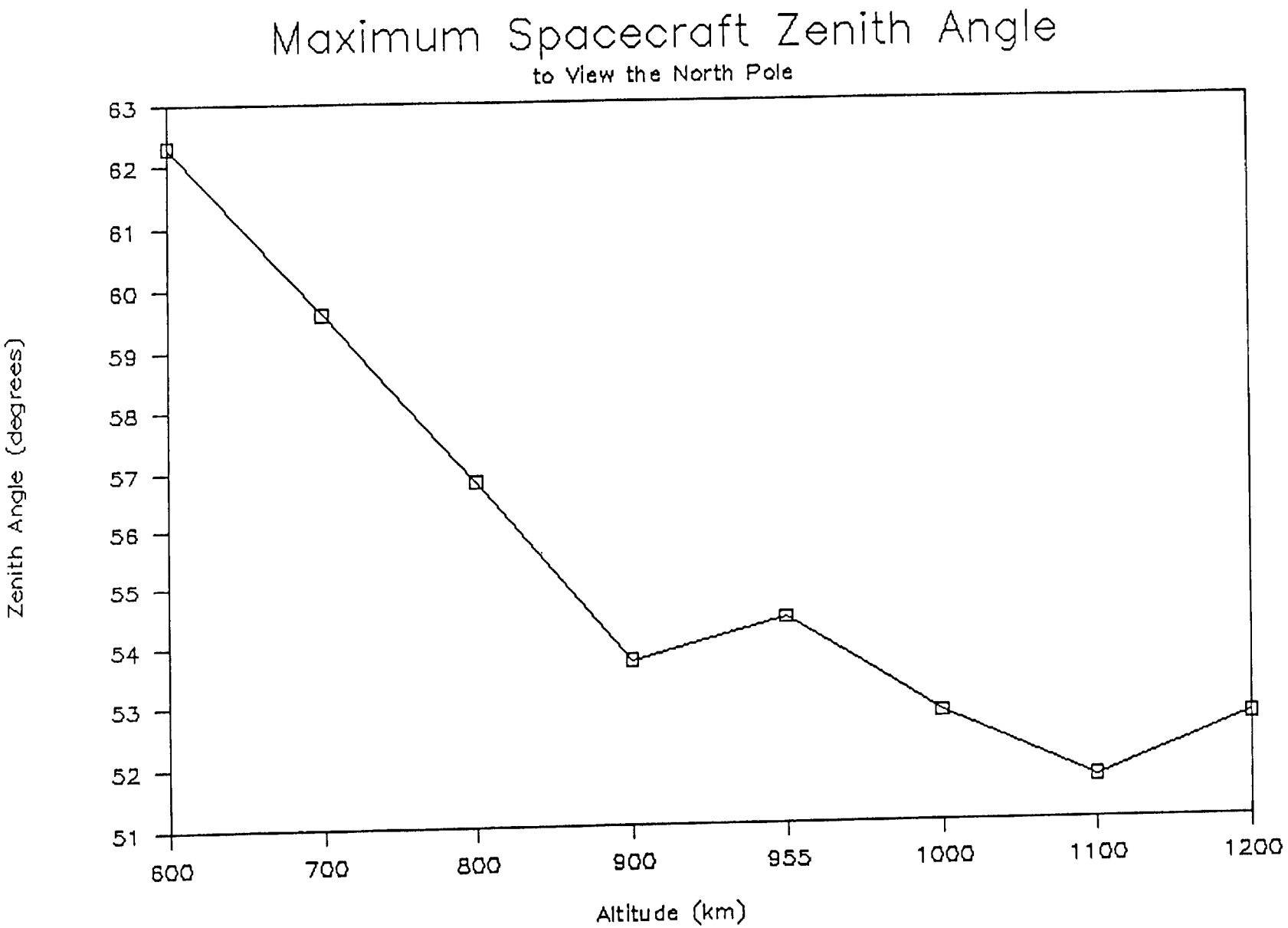

Figure 5. Maximum θ required to view the poles.

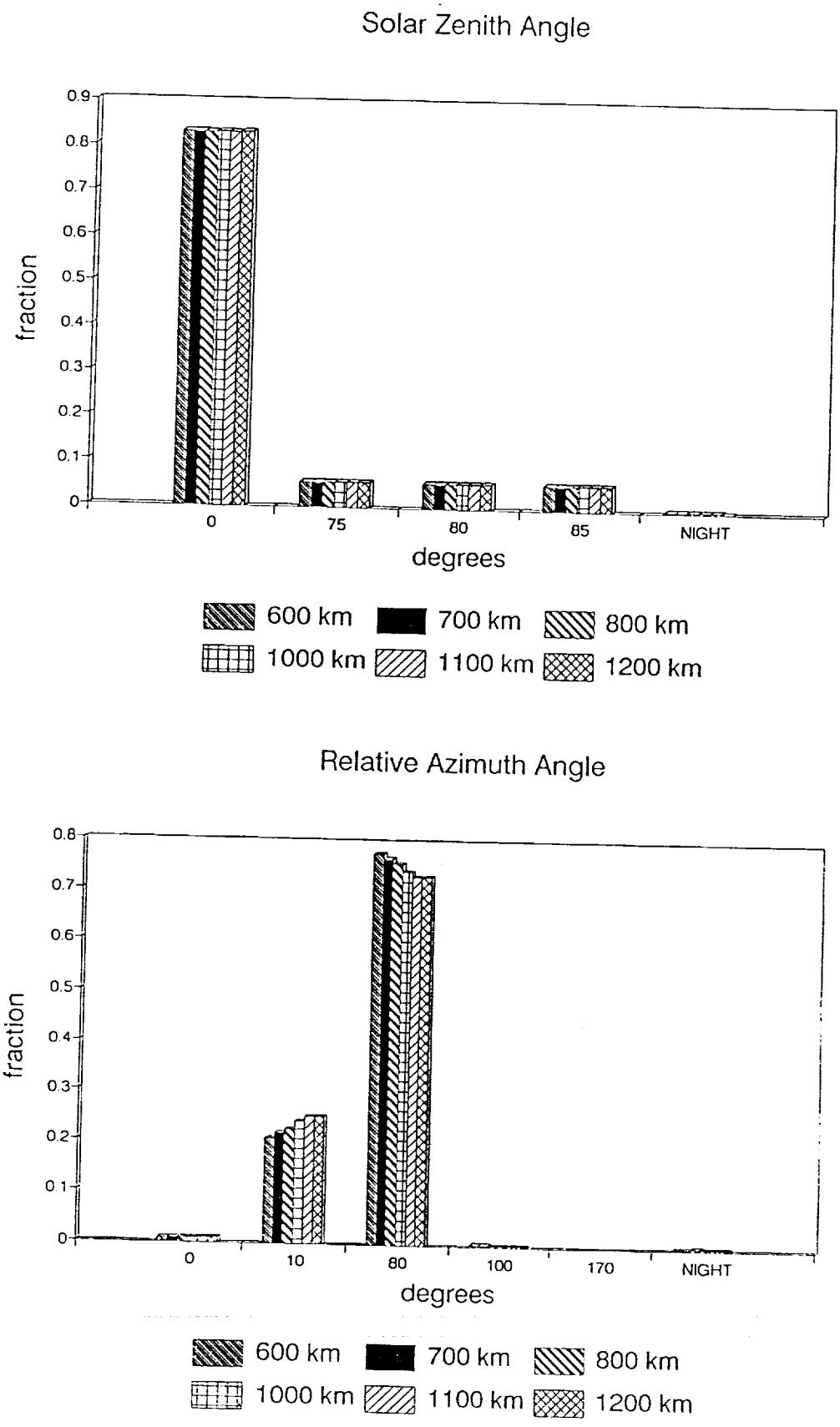

Figure 6. Histograms of the frequency of occurrence of solar zenith angles θ_o and relative azimuth angles ϕ-ϕ_o for various altitudes. Computations were made for all pixels in ascending node, from South Pole to North Pole.

Although the SCOUT will be initially launched in a near-noon ECT, as was Nimbus-7, it may drift. Nimbus-7 drifted by less than 1 hour in its 11-year lifetime. It is important to know the effects and tolerance levels of local time drift in order to place thrusters and fuel on the satellite. Analysis of the effects of ECT was restricted to the Nimbus-7 orbit (955 km) and focused on solar geometry. Along-track, across-track distributions of θ_o for the Nimbus-7 orbit are shown in Figure 7 for the equinox. The symmetry is readily apparent, although the lowest θ_o is located slightly east of center. This is due to the time correction for the θ_o computation. As noted earlier, the solar day varies in length throughout the year such that it is not directly overhead at the vernal equinox at noon (Iqbal, 1983).

For a 1:00 p.m. ECT, the subsolar point is west of the subsatellite point, producing greater θ_o at the scan center and right-hand sides, and lower θ_o at the left-hand side of the scan (Figure 7). At a 3:00 p.m. ECT, the situation is exacerbated, with θ_o nearly 45° near the center of the scan at the equator and generally much higher θ_o throughout the ascending node (Figure 7). Note also that the 90° θ_o contour line (the terminator) now appears prominently in the Southern Hemisphere south of -73° on the scan right-hand edge. Thus there is loss of daytime coverage in the Southern Hemisphere, which is required for ozone retrievals.

For a morning ECT the situation is reversed: the subsolar point is now east of the subsatellite point and at 9:00 a.m. there is loss of daytime coverage in the Northern Hemisphere. Otherwise, the patterns are simply mirror-images of the afternoon ECT's.

Similarly, there are major changes in the distribution of relative azimuth (Figure 8). There is only a small portion of the ascending node where ϕ-ϕ_o exceeds 100° (just west of the subsatellite point), while nearly all of the left-hand side of the scan exceeds 100° for a 1:00 p.m. orbit. The left-hand side of the scan for the 3:00 p.m. orbit is entirely greater than 130°.

These results suggest strongly that ECT may be an important factor in maintaining a consistent ozone time series, particularly with respect to Earth daytime coverage.

3.3 Effects of ECT on Earth Daytime Coverage

More important than the changes in solar zenith and azimuth, and their potential effect on the accuracy of ozone retrievals, is the loss of daytime coverage by the different ECT's. For this analysis, daytime was considered as those pixels where θ_o was $\leq 88°$ (the highest θ_o useable in the ozone algorithm). The entire ascending node was simulated; if any pixel in any scan contained $\theta_o \leq 88°$, the entire latitude (in 1° bins) containing the pixel was assumed covered in daylight. This analysis was run over the course of the year to show the changes in daylight coverage as a function of the solar declination.

Daytime coverage for noon ± 3 hours ECT is shown in Figure 9, where the diamonds denote the afternoon (3:00 p.m.) ECT and the upside-down triangles, the morning (9:00 a.m.) ECT. Noon ECT is the solid line, which forms the boundary for the coverage plot. As expected, there was no daytime coverage of the Antarctic during the Southern Hemisphere winter (Julian Day 100 - 250) nor of the Arctic during the Northern Hemisphere winter (Julian Day 290 - 60) for any ECT.

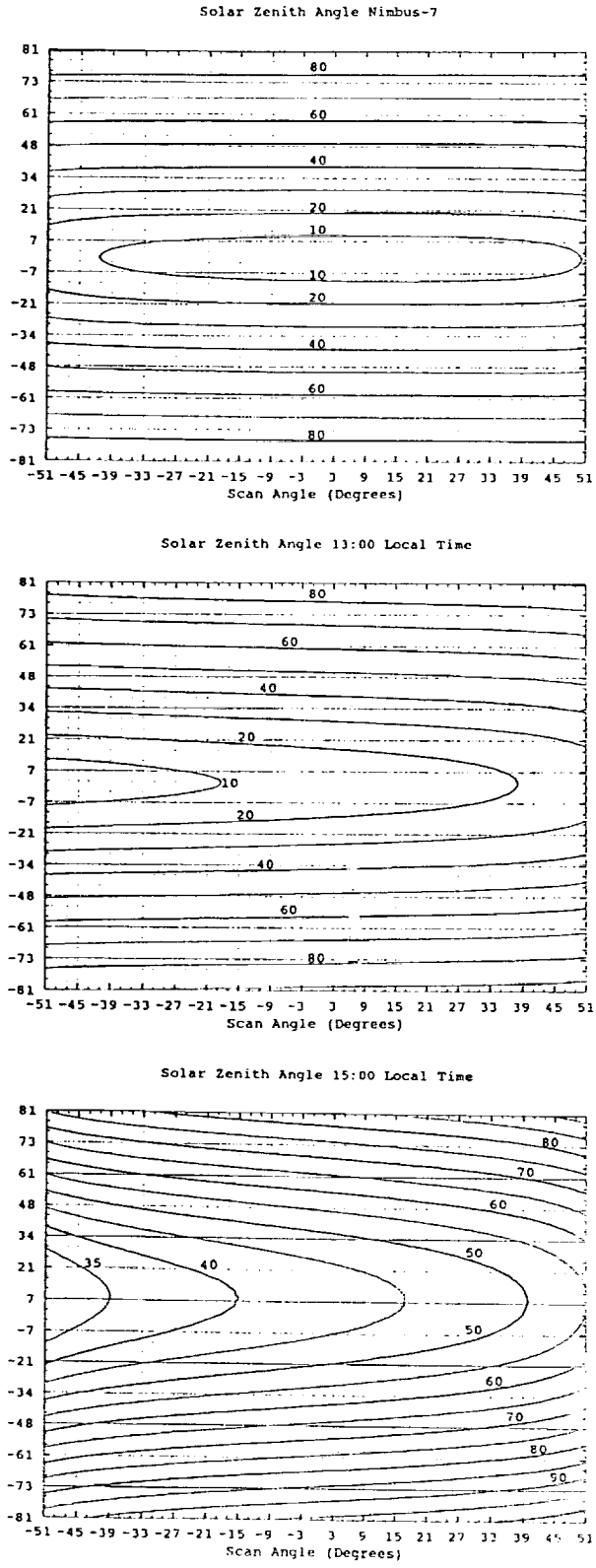

Figure 7. Along-track, across-track distribution of solar zenith angles in ascending node from South Pole to North Pole. The y-axis denotes latitude. Top: Nimbus-7 (noon local equator crossing time). Center: 1:00 p.m. equator crossing time. Bottom: 3:00 p.m. equator crossing time.

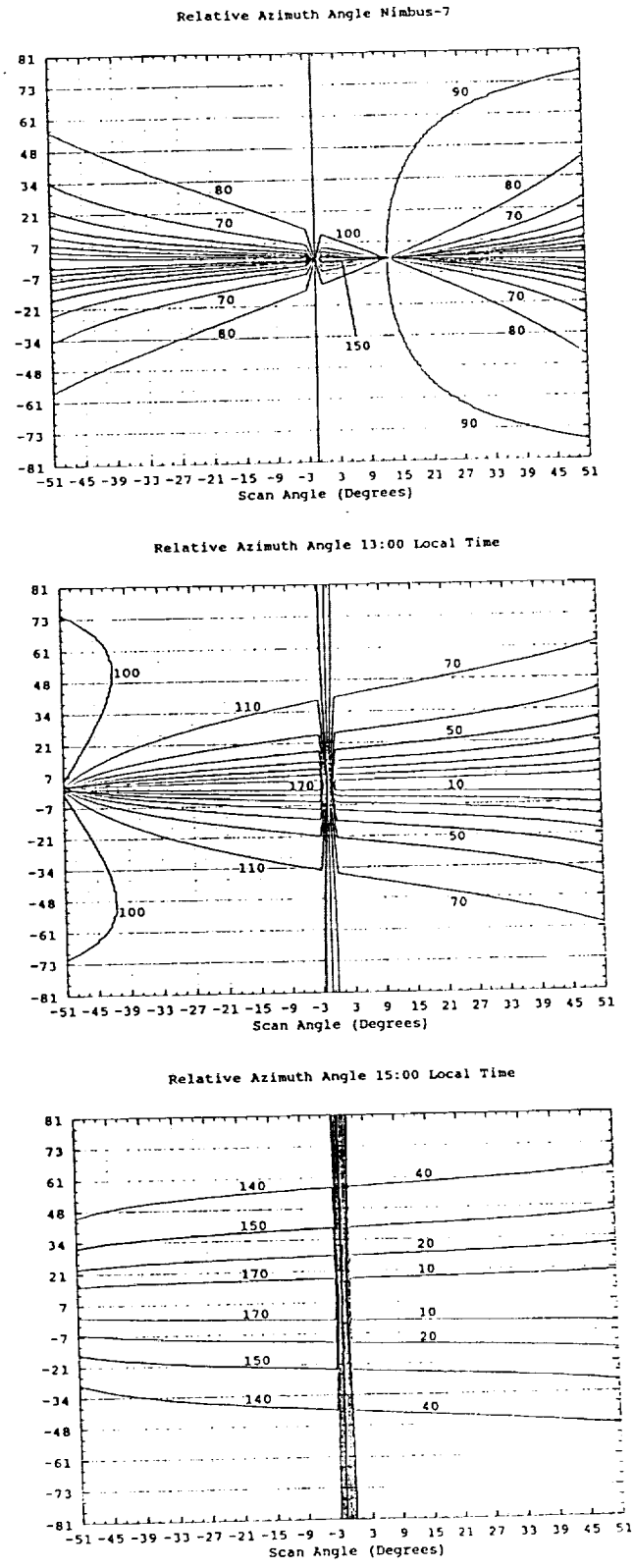

Figure 8. Along-track, across-track distribution of relative azimuth angles in ascending node from South Pole to North Pole. The y-axis denotes latitude. Top: Nimbus-7 (noon local equator crossing time). Center: 1:00 p.m. equator crossing time. Bottom: 3:00 p.m. equator crossing time.

However, the afternoon orbit resulted in decreased coverage relative to the noon orbit in the Southern Hemisphere, but no change in coverage occurred in the Northern Hemisphere (Figure 9). The reverse situation occurred with respect to the morning orbit--decreased daytime coverage of the Northern Hemisphere and no change in the Southern. This is due to the inclination of the Sun-synchronous orbit: the inclined orbits travel South to North, but are east of the equator crossing longitude in the Southern Hemisphere (and in afternoon local time for a noon ECT), and west of the equator crossing longitude in the Northern Hemisphere (and therefore in morning local time for a noon ECT). For a morning ECT, the subsolar point is located east of the equator crossing longitude, and therefore actually closer to the easterly position of the subsatellite track in the Southern Hemisphere. Thus no change in Southern Hemisphere daytime coverage results from a morning ECT. However, in the Northern Hemisphere, the westerly track of the subsatellite track places the orbit even further away from the subsolar point than the noon orbit (local time is earlier in the morning), thus resulting in a loss of coverage. The reverse situation occurs with respect to an afternoon orbit--the subsolar point is farther away from the subsatellite track in the Southern Hemisphere, thus placing the pixels in later afternoon and resulting in loss of coverage. But no coverage loss is observed in the Northern Hemisphere. This is a matter of ground distance between the subsolar and subsatellite points. It should be noted that the noon ECT produces the maximum daytime coverage for any day of the year.

If more extreme examples of ECT's are examined, it is seen that at ± 6 hours from noon, there is significant daytime coverage loss in the Southern Hemisphere for a morning orbit and in the Northern Hemisphere for an afternoon orbit (Figure 10). But the coverage losses in the opposite hemisphere are now extremely pronounced--loss in the Southern Hemisphere extends to nearly -20°S for a 6:00 p.m. ECT and in the Northern Hemisphere to 20°N for a 6:00 a.m. ECT.

In an effort to quantify these daytime coverage losses due to ECT and to find the limits of acceptability, the loss in coverage was computed from a noon ECT in degrees latitude. Two plots are presented, one for Southern Hemisphere loss due to afternoon ECT's, and one for Northern Hemisphere loss due to morning ECT's. Recall that these scenarios emphasize the maximum in coverage loss.

Figure 11 shows that 6° latitudinal daytime coverage loss occurs for ECT's within 3 hours of noon. Coverage loss increases rapidly each hour outside this limit, eventually reaching nearly 53° coverage loss for 6:00 a.m. and 6:00 p.m. ECT's. Loss is minor ($< 5°$) for ECT's within 2 hours of noon. These results suggest that orbit drift to noon ± 2 hours ECT may be acceptable, but that departures from noon produce substantial daytime coverage loss. Departures greater than ± 3 hours from noon ECT must be avoided.

3.4 Effects of Elliptical Orbits on Earth Daytime Coverage

The scan period of the Nimbus-7 TOMS (8 sec) was designed to maintain contiguous Earth coverage along-track. This scan period was determined by knowledge of the ground speed and IFOV of the spacecraft. The SCOUT/TOMS may be placed in a temporary transfer elliptical orbit before proceeding to a circular one. For an elliptical orbit, the ground speed will change along orbit: at perigee the ground speed will be greater and at apogee it will be less. This fact,

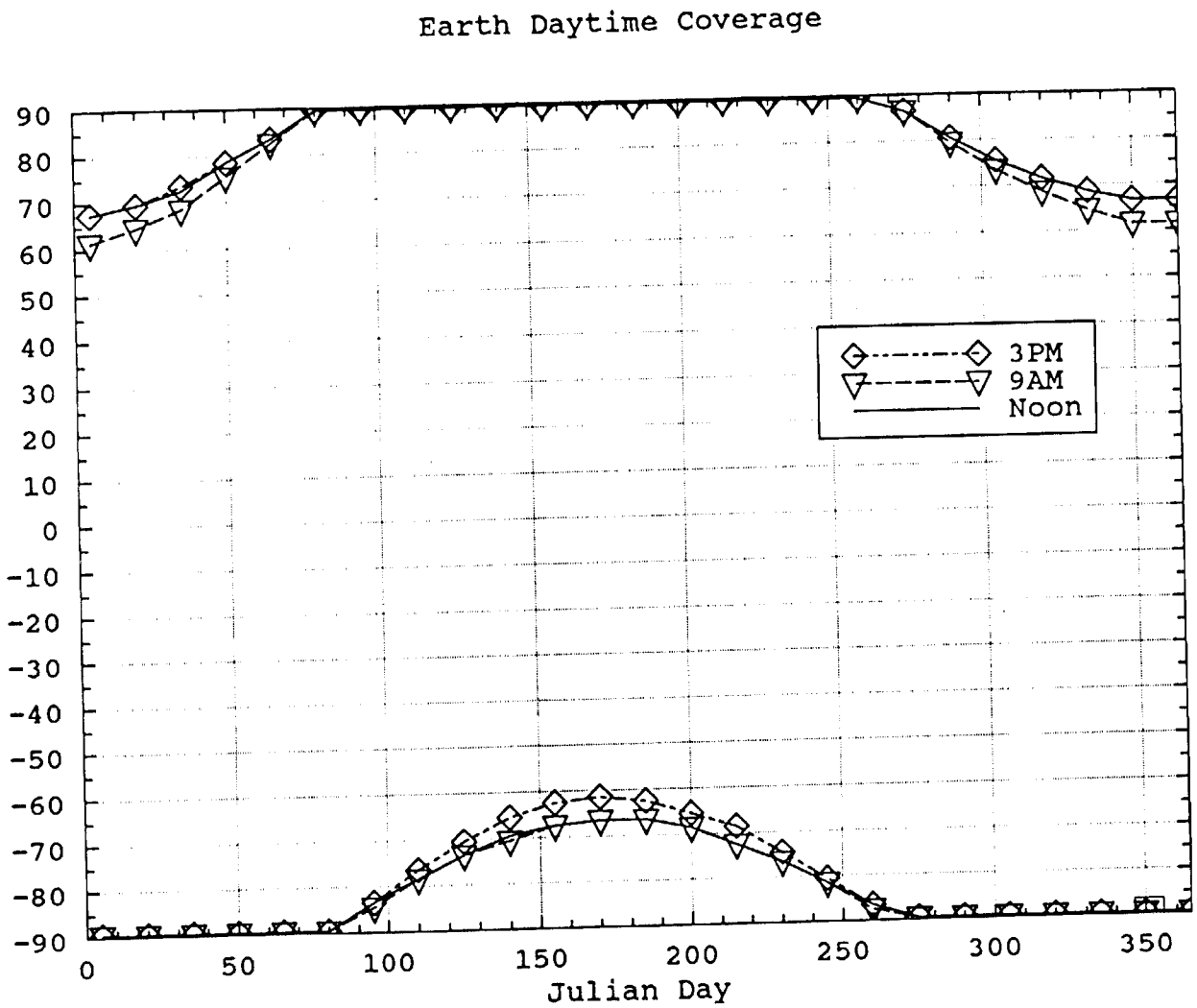

Figure 9. Earth daytime coverage as a function of equator crossing time, for noon ±3 hours. Daytime is defined as those areas where the solar zenith angle is greater than 88°.

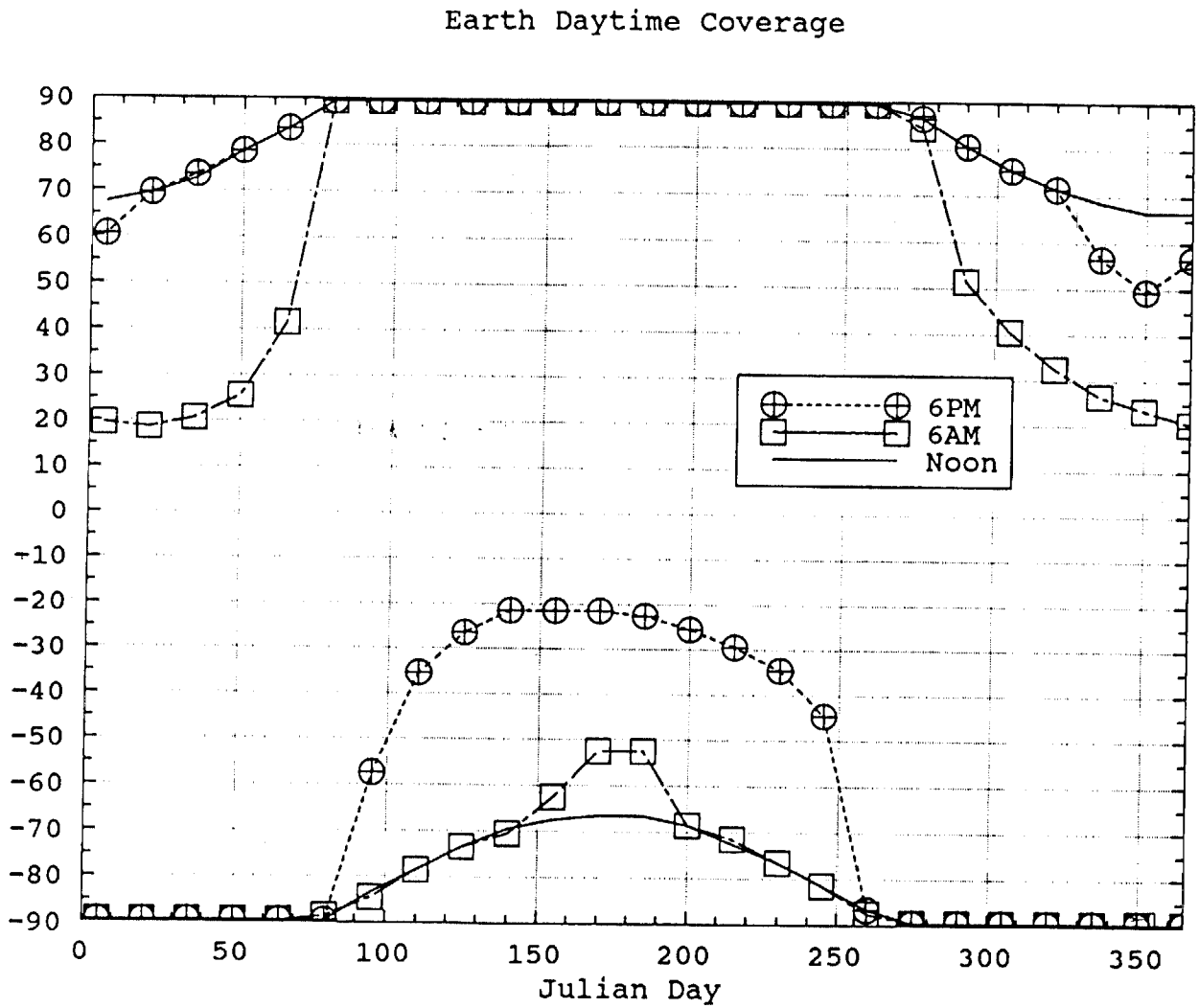

Figure 10. Earth daytime coverage as a function of equator crossing time, for noon ±6 hours. Daytime is defined as those areas where the solar zenith angle is greater than 88°.

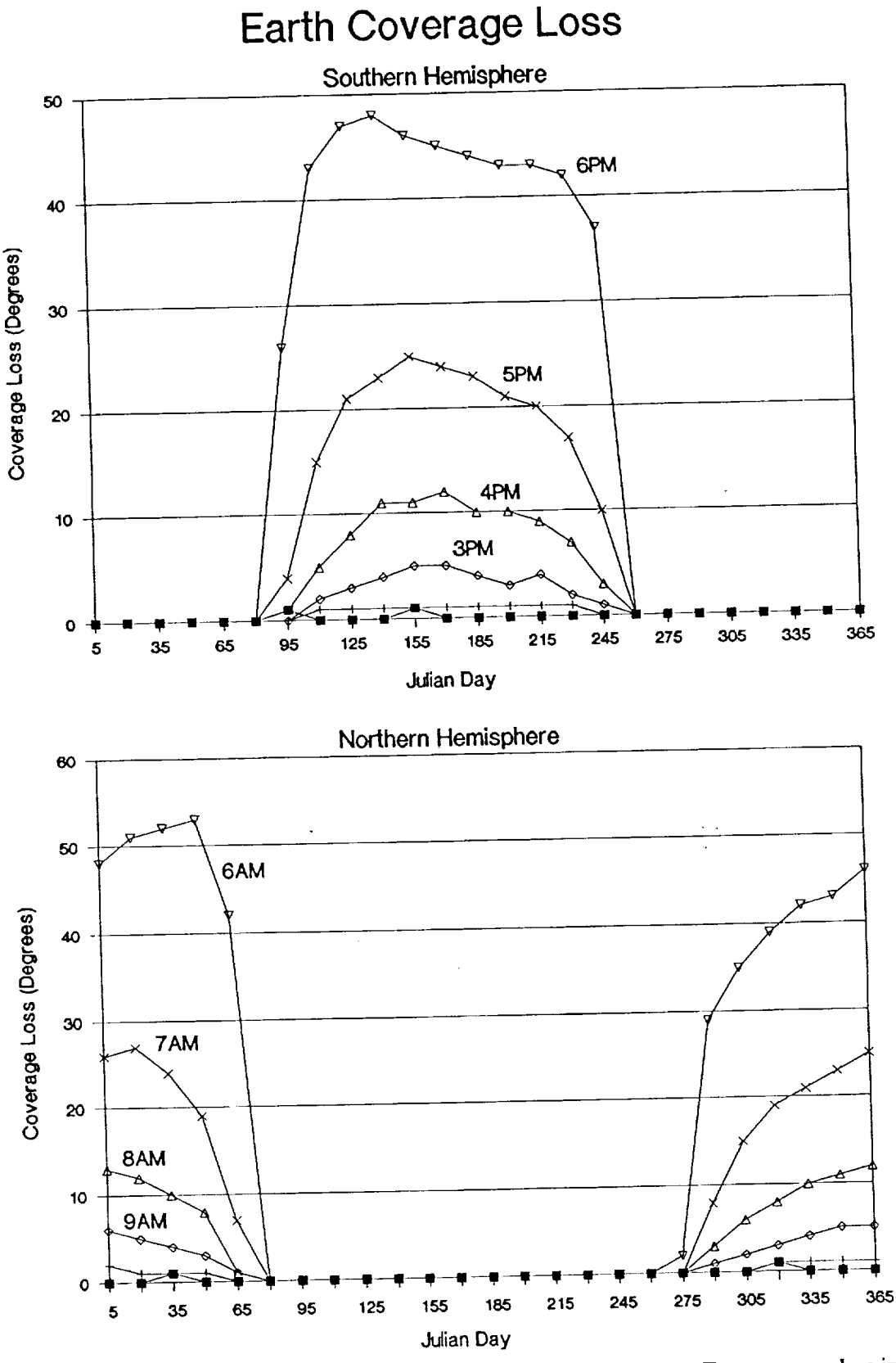

Figure 11. Earth daytime coverage loss relative to a noon equator crossing time. Top: coverage loss in the Southern Hemisphere resulting from afternoon ECT's. Bottom: coverage loss in the Northern Hemisphere resulting from morning ECT's.

coupled with a reduced ground IFOV at perigee, will affect the Earth coverage if the scan period remains fixed.

In the simulations presented here, it is assumed that the SCOUT/TOMS will be designed for a Nimbus-7 type orbit--circular at 955 km. The effect of elliptical orbits on Earth coverage due to the changing ground speed and ground IFOV is investigated for a fixed scan period of 8 sec.

The maximum ground speed and minimum ground IFOV is attained at perigee for an elliptical orbit. Thus the maximum coverage loss will occur at perigee. Furthermore, because of slant path length considerations and the widening of pixel areas, the maximum loss will be at nadir. Ground speeds at perigee for several elliptical orbit scenarios are shown in Figure 12. The maximum occurs at perigee for the 200- to 1200-km orbit, at 8.5 km s^{-1}, and linearly decreases for the remaining scenarios.

The associated coverage loss at nadir is shown in Figure 12, where a maximum loss is attained at the 200- to 1200-km scenario (45 km), and the minimum at 955 km circular (0 km--no loss). A linear trend in coverage loss is apparent for the other elliptical scenarios.

There is no loss in coverage at apogee--in fact, there is increased overlap for an apogee at 1200 km. However, any portion of the orbit where the altitude is <955 km will result in loss of coverage, if the scan period remains fixed.

This maximum coverage loss at perigee will not occur at the same location on the Earth, since the perigee moves opposite the direction of the satellite motion. The rate is approximately 3 degrees day^{-1} for a 400- to 955-km orbit. This means that if the perigee first occurs at the South Pole, it (and the coverage gap associated with it) will move to the equational region in a month. The impact of this is that at crucial times TOMS will miss areas for as long as a few months.

3.5 Error in Ozone Retrieval Due to Attitude Uncertainty

Specifications for the TOMS/SCOUT mission include a 0.1° attitude knowledge requirement. This requirement is on each axis (pitch, roll, yaw) independently. Here the impact of the attitude uncertainty on the retrieval of ozone is investigated using the TOMS ozone retrieval algorithm.

Recall that the maximum errors were simulated: a viewing geometry required for North Pole coverage, attitude configuration within the 0.1° specifications to produce the maximum error, and on the day of year when errors were maximum. Thus the analysis is for a worst-case scenario.

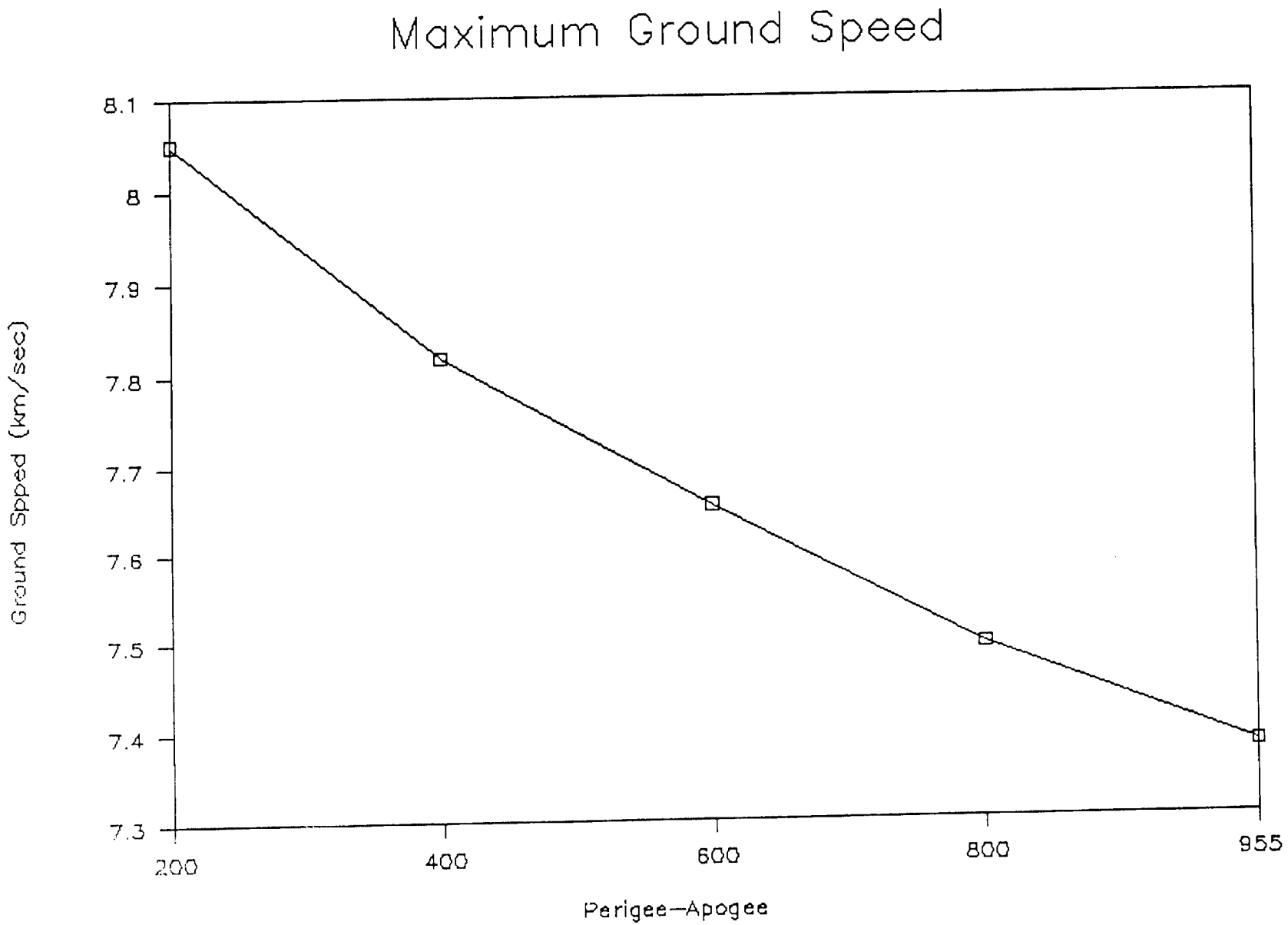

Figure 12. Maximum ground speeds and associated Earth coverage losses at perigee for several elliptical orbits.

For the Nimbus-7 (955-km) orbit, the maximum errors in retrieved ozone due to attitude uncertainty were:

Low Ozone (130 DU)	0.59 DU (0.45%)
Medium Ozone (320 DU)	1.13 DU (0.87%)
High Ozone (570 DU)	1.26 DU (0.22%)

In each case the attitude perturbation produced a slightly higher estimate of ozone, and the error was thus positive. The error for the medium and high ozone cases exceeds the desired accuracy of 1 DU, but is a small error in percent.

The attitude uncertainty error in ozone was also examined for the other 7 orbit scenarios, again all at the North Pole viewing geometry. The changes (increase or decrease) in error from that at the Nimbus-7 orbit are shown in Figure 13. Errors due attitude uncertainty were generally small, never exceeding 1.5 DU even under the worst conditions simulated here.

The relative ozone error due to attitude uncertainty was computed by dividing the error at a given altitude by that at 955 km (Figure 13). Values less than 1 indicate a decrease in the error due to attitude uncertainty relative to Nimbus-7, while values greater than 1 indicate an increase. Clearly, the lower altitude orbits produced less ozone error due to attitude uncertainty, while the high altitude orbits produced greater error. This suggests greater sensitivity of higher altitude orbits to attitude perturbations.

These results are because for lower altitude orbits, a small change in attitude produces a smaller change in pointing direction (and in solar and viewing geometries) than for high altitude orbits. Thus higher altitude orbits are more sensitive to attitude perturbations than are lower altitude orbits. Lower altitude orbits reduce the sensitivity of the ozone retrieval algorithm to attitude uncertainty.

Regardless, however, it must be emphasized that the errors are small even under these simulated worst-case conditions. The conclusion drawn from these analyses is that orbital altitude makes negligible difference in ozone retrieval, given an attitude knowledge of 0.1° in each axis.

Errors were also examined for an attitude perturbation of 1° in each axis. The errors appeared to be linear, increasing to ≈ 10 times the value at 0.1°. These new errors at an uncertainty of 1° were: low ozone = 5.95, medium ozone = 11.51, high ozone = 12.84 DU. These analyses had to be performed one day earlier than the 0.1° analyses because the 1° attitude perturbation resulted in a solar geometry greater than the 88° threshold.

3.6 Error in Ozone Retrieval as a Function of Altitude

The changes in viewing geometry (specifically the spacecraft zenith angle) due to orbital altitude suggest that altitude may affect the retrieval of ozone. This is critical to maintain a coherent time series of ozone data to understand long-term trends in ozone. However, changes in viewing geometry do not by themselves demonstrate a degradation of ozone retrieval. It is thus necessary to understand how these geometrical considerations relate to ozone retrievals.

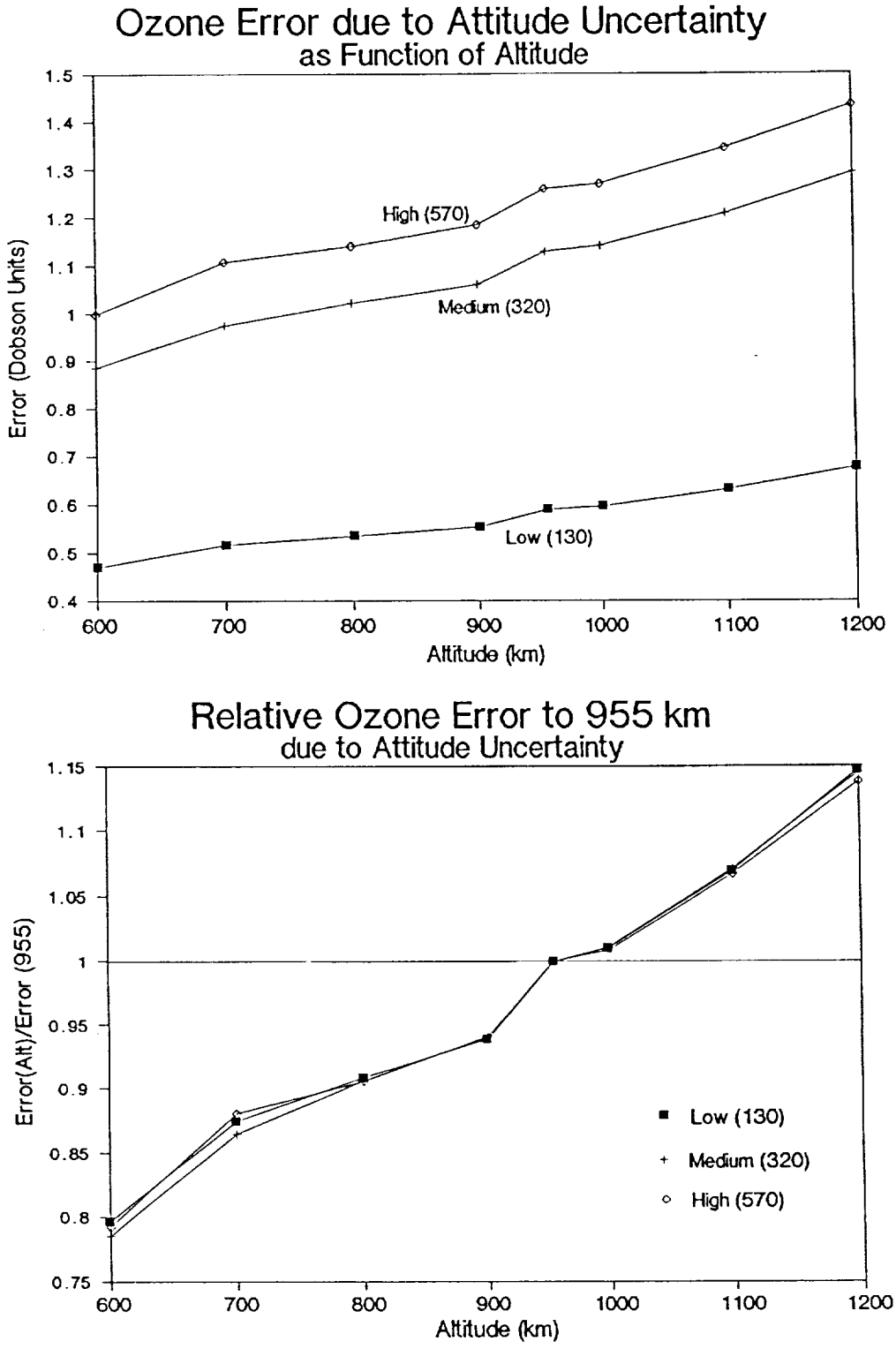

Figure 13. Ozone error due to attitude uncertainty as a function of altitude, for three ozone values. Errors were determined for a viewing geometry required to observe the North Pole, at maximum attitude perturbation (within 0.1° in each axis), on the day of year of maximum error. Top: absolute errors. Bottom: errors relative to those at 955 km.

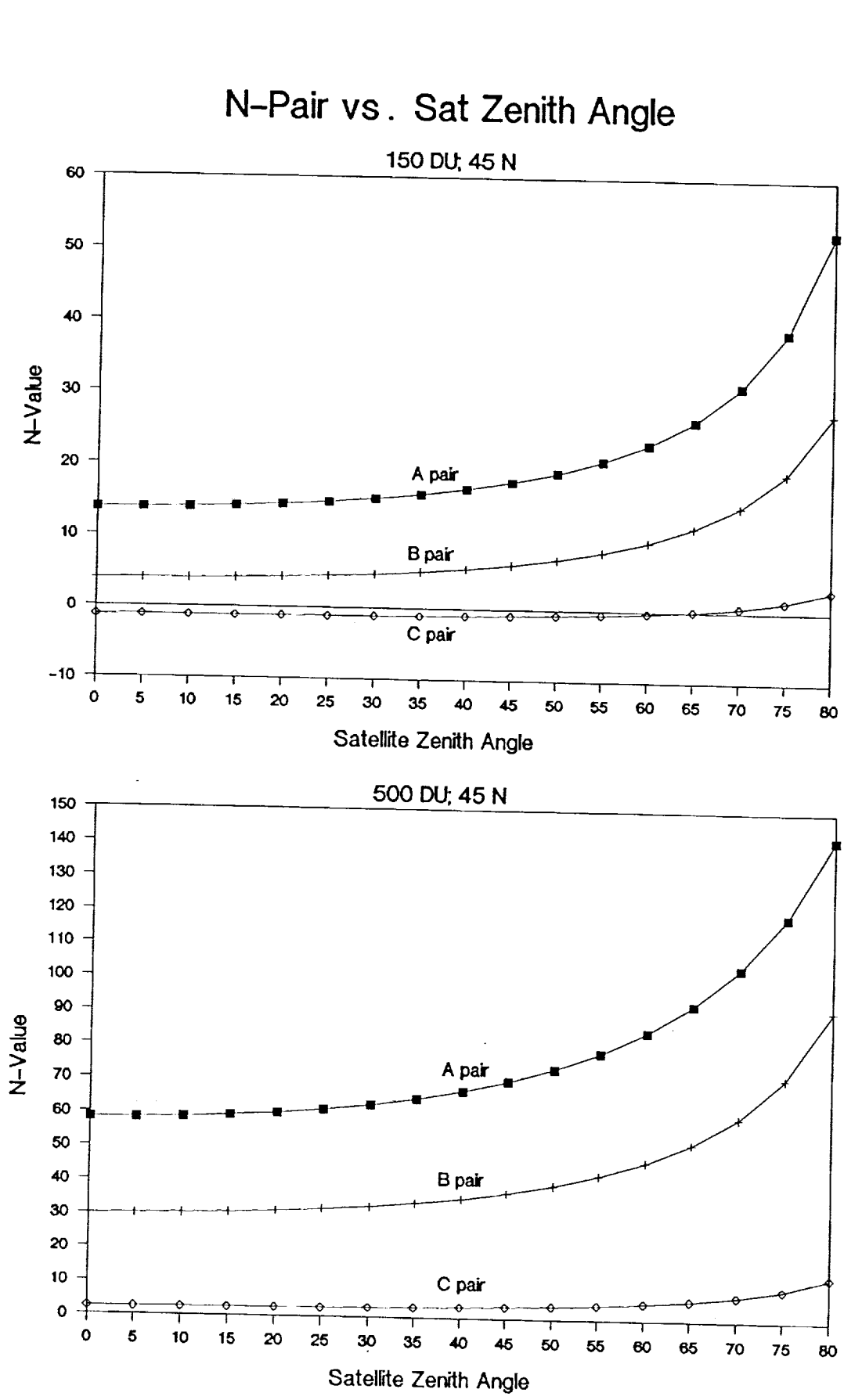

Figure 14. Sensitivity of ozone N-Tables to spacecraft zenith angle for low ozone (150 DU) and high ozone (500 DU) at 45°N. The solar zenith angle in these cases was 30°, with a relative azimuth of 90°.

It has been shown how altitude affects θ at the equator and poles, and that it has no effect on θ_o and only minor effect on ϕ-ϕ_o. The question here is: how do these changes in θ relate to ozone retrieval? A partial answer to the question may be inferred from Figure 14, which shows the changes in the ozone N-pairs with θ. This is essentially a plot of $\Delta N_i/\Delta\theta$, where the subscript i denotes the N-pair A, B, or C. Three ozone values are depicted; 150, 300, and 500 DU.

Over the range $0° < \theta < 40°$ there is very little change in N_i, but for $\theta > 60°$ the relationship is decidedly nonlinear, especially for N_a and N_b. These results suggest that the ozone algorithm is insensitive to changes in θ for angles $< 40°$, but may be sensitive to angles $> 60°$. Recall that the range of θ to view the North Pole was from $\approx 62°$ at 600 km to 51.5° at 1200 km. This range of θ is in the region of the $\Delta N_i/\Delta\theta$ where the relationship is slightly nonlinear. Thus, one must conclude that the range in θ incurred by these altitudes may be important in the retrieval of ozone.

However, a quantitative estimate of the error in ozone retrieval due to altitude is still undetermined. To address this question, the profile uncertainty was used to estimate the error in ozone due to altitude, through the changes in θ. Again three ozone amounts were used; low (130 DU), medium (320 DU), and high (570 DU) ozone. These values may be compared to the figures of θ at the equator and to view the North Pole (Figures 4 and 5).

Baseline values were obtained by performing this procedure for the Nimbus-7 (955 km) orbit. RMS errors due to profile uncertainty are shown in Table 10.

Table 10. RMS Error in Dobson Units (Maximum Error in Parenthesis) Due to Ozone Profile Uncertainty at 955 km for Three Latitude Regions and Three Ozone Amounts

The sign in the RMS errors denotes whether this is an underestimate or overestimate: underestimate is negative

	Equator	Mid-Latitude	Pole
Low Ozone	--	2.4 (-2.7)	2.1 (2.3)
Medium Ozone	-2.1 (-2.3)	-8.2 (-21.4)	14.9 (52.7)
High Ozone	--	-1.8 (2.2)	1.3 (2.3)

A very large error due to profile uncertainty is apparent for medium ozone at mid-latitudes and the poles. Errors elsewhere were fairly small, especially in percentage. No attempt was made to compute error for low or high ozone at the equator because of a lack of physical realism here.

This error was expressed as a function of altitude as shown in Figure 15. Only the medium ozone is shown, since the errors for other ozone amounts were small. For all altitudes, the error was high at mid-latitude and the pole. The error due to profile uncertainty was smaller at low latitude but approached 5 DU at 600-km altitude.

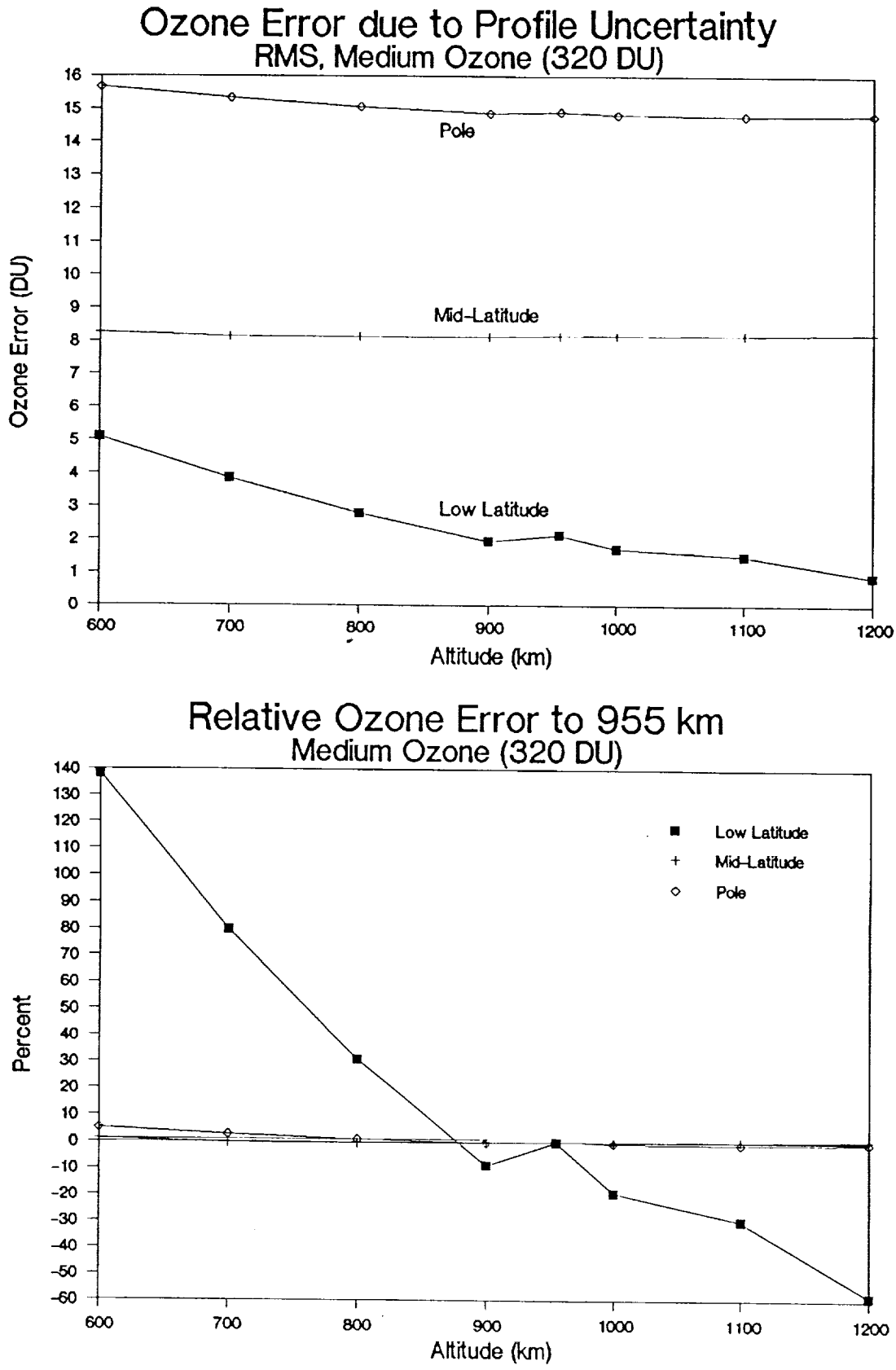

Figure 15. Ozone error due to ozone profile uncertainty as a function of altitude for medium ozone. Top: RMS errors. Bottom: Relative RMS errors to 955-km orbit.

Change in error as a function of altitude was computed as a percent at different orbital altitudes relative to the error at 955 km (i.e., relative error). These changes are plotted in Figure 15 for the medium ozone amount. The increase in error for medium ozone at 600 km was 140% greater than that at 955 km at the equator. The error decreased with increasing altitude, becoming smaller than the error at 955 km at altitudes > 1000 km. The error was small at mid-latitude and the pole.

The changes in error due to altitude are due entirely to the change in θ. Thus altitude can seriously affect ozone retrievals due to changes in θ. A 600-km orbit can increase the error due to profile uncertainty by as much as a factor of 2.5 at the equator. Higher orbits have little effect as long as the orbits are Sun-synchronous and near-noon local time. In fact, at altitudes greater than 955 km, the ozone profile uncertainty error was actually smaller than at 955 km at the equator.

The high and low ozone amounts indicated very little error due to profile uncertainty at any latitude. The medium ozone exhibited the largest error because it is this profile that changes the most from latitude bin to latitude bin.

3.7 Error in Ozone Retrieval as a Function of ECT

As a final analysis, attention is turned to the ozone errors incurred by changing ECT. The loss in Earth daytime coverage due to ECT is noted, but now the examination of the effects of ECT on ozone retrievals through changing θ_o is desired. This analysis follows the same procedure as is used in the altitude errors section, using the ozone profile uncertainty as the means to assess errors in algorithm retrievals. However, this time the ECT is changed and spacecraft geometry is fixed. Thus, the only variables are the solar zenith and relative azimuth angles. Again for this analysis, we computed RMS errors over the year to take into account the changing solar position through the year. However, because of pronounced asymmetries in the error distribution, the left-most pixels in the sensor scan were examined in addition to the right-most pixels.

As with altitude, the greatest errors in ozone retrieval due to profile uncertainty occurred for medium ozone for all three latitudes (Figure 16), where errors up to 18 DU were attained for mid-latitude at a 10:00 a.m. ECT. Errors did not exceed 2.5 DU for the low and high ozone amounts at any latitude.

At the equator, errors were greater for afternoon ECT's than for morning ECT's for the right-most pixel, which is closer to the subsolar point in the morning than in the afternoon, resulting in a lower θ_o. The reverse pattern occurred with respect to the left-most pixel, which attained maximum error for a morning ECT. An interesting event is the location of the minimum error. For the right-most pixel, the minimum occurred at 1:00 p.m., rather than at 11:00 a.m., when the solar position is closest to the pixel. Figure 17 shows the subsolar positions throughout the year relative to the right-most pixel at the equator. Clearly, the subsolar positions for an 11:00 a.m. ECT are much closer to the right-most pixel than at 1:00 p.m., resulting in smaller θ_o. The key to this apparently anomalous condition is the relative azimuth. This changes only moderately throughout the year for the right-most pixel at 1:00 a.m., ranging from about -70°

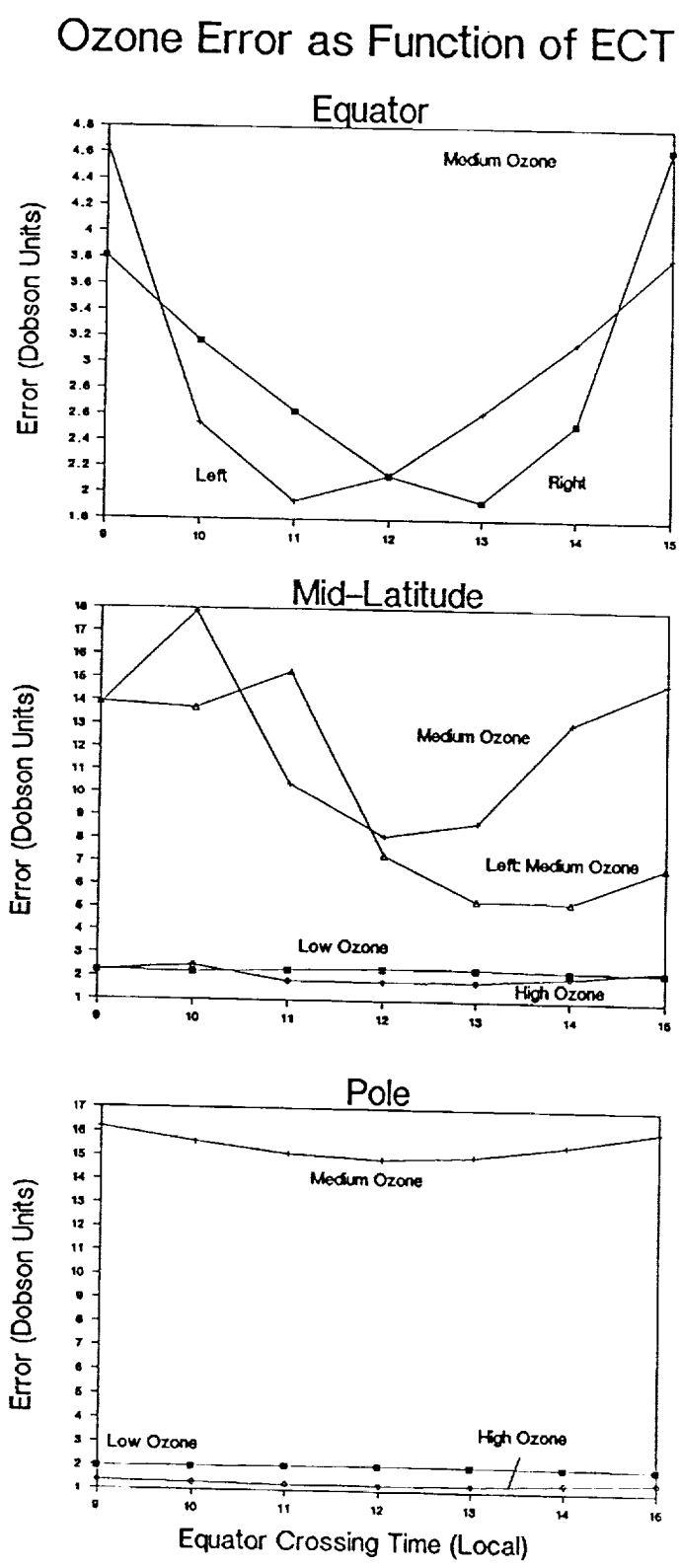

Figure 16. Ozone error due to profile uncertainty as a function of equator crossing time (ECT), expressed as RMS error throughout the year to take into account the changing solar declination. Top: an equatorial pixel. Only medium ozone is depicted because low and high ozone amounts are rare in the tropics. The higher error for an afternoon ECT is because the extreme right-hand side of the scan is simulated here. The left-hand side of the scan is shown, also, and shows the reverse pattern. Center: a mid-latitude pixel (60°N). Three ozone amounts are shown. The maximum error occurs for medium ozone (320 DU). Bottom: a polar pixel. Again the maximum error is for medium ozone.

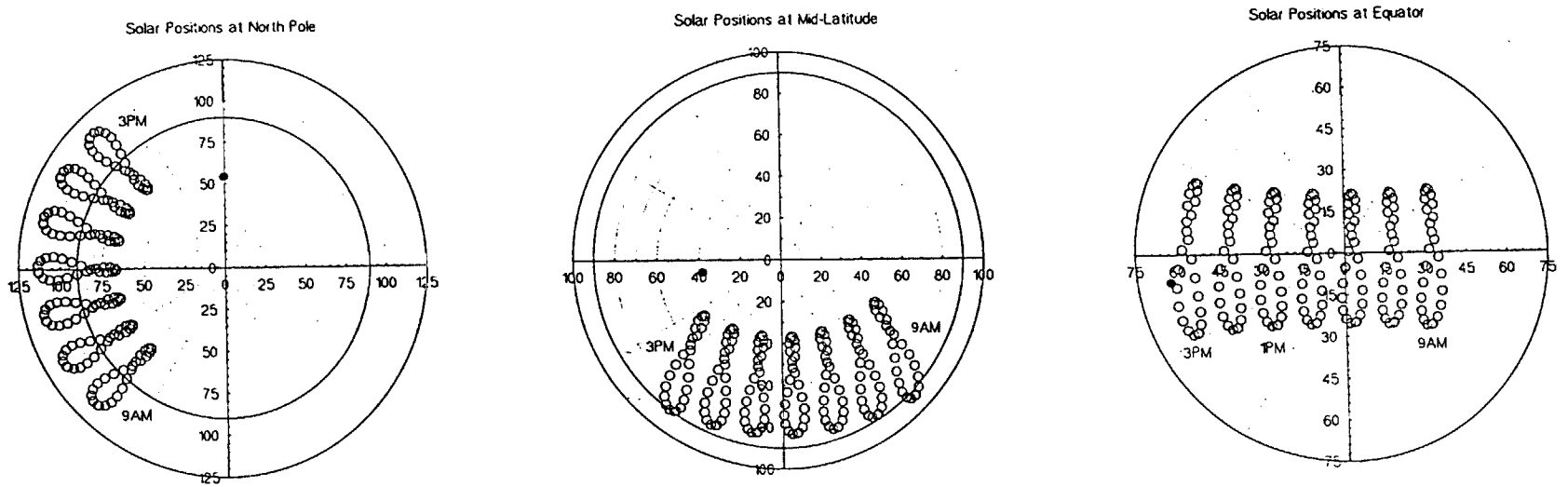

Figure 17. Subsolar positions throughout the year as seen by a pixel under observation, as a function of ECT. In these plots the right-most pixel is the target pixel, and is located at the center. Zenith angle relative to the target pixel is determined by radius, and true azimuth (measured clockwise from north -- top) is the circumference. The filled black dot is the satellite location in these zenith, azimuth coordinates. Northern Hemisphere summer is noted by the most northerly (toward the top of each plot) extent of the solar positions, winter by the most southerly (toward the bottom) positions. At the North Pole the pixel covering the pole has a center slightly over the top, so that the satellite is located due north over the pole from the pixel. These right-most pixels conform to the maximum scan position required to avoid scan overlap from preceding/succeeding orbits, as described in the text.

in the Northern Hemisphere summer to $\approx 45°$ for winter (Figure 17), an absolute range of $\approx 70°$. Conversely for an 11:00 a.m. ECT, the relative azimuth ranges from $\approx 250°$ in summer, through 180° in spring/autumn, to $\approx 80°$ in winter (Figure 17), an absolute range of $\approx 170°$. Although the dependence of the ozone retrieval algorithm to relative azimuth is small, it is about of the order of difference seen here between 11:00 a.m. and 1:00 p.m. (≈ 0.5 DU). The 11:00 AM ECT provides smaller θ_o than 1:00 p.m., but θ_o at 1:00 p.m. is not large, and the change in relative azimuth throughout the year at 11:00 a.m. is much greater, causing larger error in ozone retrieval than at 1:00 p.m. The reverse pattern occurs for the left-most pixel.

At mid-latitude, it is interesting to note the maximum error at 10:00 a.m. ECT rather than at the extreme ECT's simulated here (Figure 16). Again referring to Figure 17, at 9:00 a.m. and 3:00 p.m., a substantial number of solar positions exceed the 88° threshold for θ_o for application of the algorithm. Thus these data are not included in the RMS error results. In contrast, all of the solar positions at 10:00 a.m. are within the threshold, and are thus included in the analyses. A very large number of these positions occur at very high θ_o ($>85°$), and the large error in ozone in the algorithm at these times weighs very heavily in the final RMS errors. Thus the error at 10:00 a.m. exceeds the more extreme 9:00 a.m. ECT because of exclusion by the algorithm.

Finally, one may note the relatively small dependence of ozone error on ECT at the North Pole (Figure 16). At this location, θ_o does not change as a function of ECT throughout the year (Figure 17); only the relative azimuth changes. As noted before, these changes produce errors of the order of 0.5 DU. This is about the range in error observed at the pole as a function of ECT (Figure 16).

Relative errors to a noon ECT (Figure 18) reflect the RMS errors depicted in Figure 16. Generally, errors due to profile uncertainty reached a minimum at or very near the noon ECT for most cases. The exception was for low ozone, which surprisingly attained maximum at noon. At mid-latitude, errors for medium and high ozone reached a maximum at 10:00 a.m. ECT, where they were 2.2 and 1.4 times the error at noon. This resulted in an increase in error of nearly 10 DU for the medium ozone case. As noted earlier, the maximum at 10:00 a.m. rather than 9:00 a.m. is a consequence of Earth daytime coverage and the 88° algorithm threshold for θ_o.

These results suggest that ECT not only affects Earth daytime coverage, as seen in Figures 9, 10, and 11, but also the retrieval of ozone as estimated by the profile uncertainty. Thus, although the change in ECT from noon ± 3 hours did not change Earth coverage significantly, it did introduce potential error in the retrieval of ozone. This may produce a bias in ozone observations, decreasing the reliability of obtaining unaliased long-term trends.

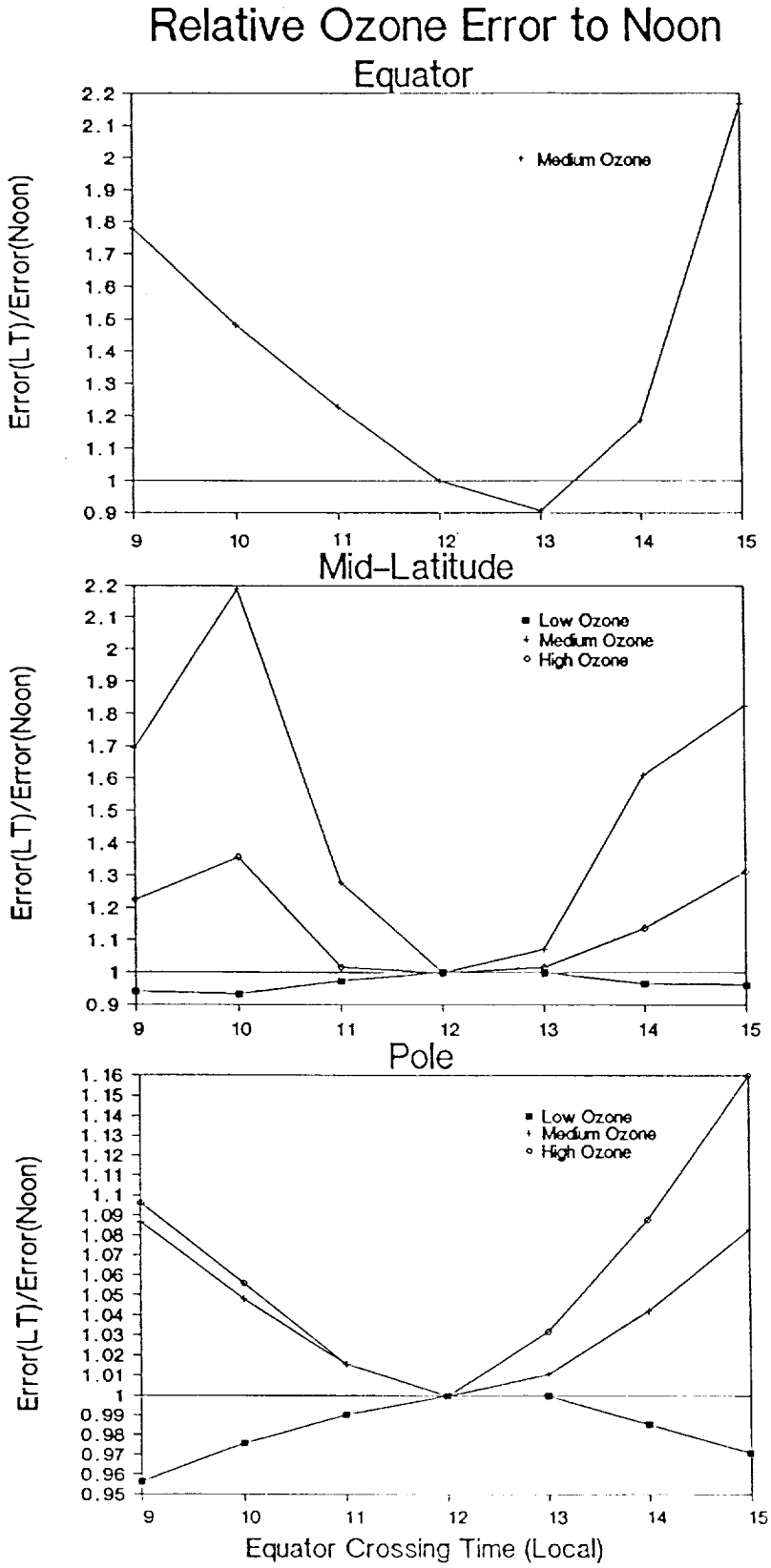

Figure 18. Relative error in ozone compared to a noon ECT. Noon represents the minimum for medium and high ozone, but the maximum for low ozone.

4.0 CONCLUSIONS

Extensive simulations of various orbital scenarios were performed to assess the potential impacts of candidate launch vehicles for a proposed follow-on TOMS sensor. Specifically examined were the effects of 1) orbital altitudes on solar and viewing geometry and ozone retrieval accuracy, 2) ECT on solar geometry, Earth daytime coverage, and ozone retrieval accuracy, 3) attitude uncertainty on ozone retrieval accuracy, and 4) orbital eccentricity on Earth daytime coverage.

The error in ozone retrieval due to profile uncertainty and loss of Earth daytime coverage associated with ECT was of paramount importance. In order to maintain a continuous, long-term ozone time series, it is critical that the ECT be kept close to noon (local time). ECT's within ± 1 hour of noon are acceptable ($\approx 1°$ latitudinal coverage loss), but those greater than ± 2 hour of noon should be avoided ($\approx 6°$ loss of latitudinal coverage at ± 3 hours). The loss of coverage associated with ECT's $> \pm 6$ hours of noon is so extensive ($\approx 53°$ in latitudinal coverage) that these crossing times must be prevented. The effects of changing altitude are less important, and altitudes greater than or equal to 800 km will produce errors relative to Nimbus-7 (955 km) of less than 1 DU. An altitude of 600 km, however, can produce errors in ozone retrieval of up to 3 DU in the worst case, and thus is less desirable.

Although changing the ECT less than ± 3 hours from noon produced small change in Earth daytime coverage, it did result in an increase in ozone error due to profile uncertainty. The minimum error occurred for noon ECT's, except in the case of low ozone. The error reached a maximum of 10 DU for medium ozone at a 10:00 a.m. ECT, compared with a noon ECT. The error for medium ozone at the equator increased by ≈ 3 DU at a 3:00 p.m. ECT compared with noon. For other ozone amounts and latitudes, the change in error was less than 1 DU compared to noon.

To maintain contiguous Earth coverage, the maximum scan angle of the sensor must be increased with decreasing orbital altitude. The maximum scan angle required for full coverage at the equator varies from 60° at 600-km altitude to 45° at 1200 km. The increase in scan angle produces an increase in spacecraft zenith angle θ, which decreases the ozone retrieval accuracy. The range in θ was $\approx 72°$ for 600 km to $\approx 57°$ at 1200 km. However, because of scan overlap between adjacent orbits, the highest spacecraft zenith angles are required only at the equator. Despite overlap, there is a unique scan angle required to view the poles for each altitude. The θ associated with these scan angles ranged from 62.5° at 600 km to 52° at 1200 km.

These changes in spacecraft zenith angle due to altitude resulted in greater than a factor of two (138%) increase in RMS error due to ozone profile uncertainty in the TOMS ozone retrieval algorithm at an altitude of 600 km, or nearly 3 DU. Altitudes greater than or equal to 900 km produced errors that did not exceed the error at 955 km by more than 10% (< 1 DU), and often produced less error than at 955 km.

Loss of Earth coverage due to orbital eccentricity may be important, especially for extreme cases. A 45-km gap in coverage at nadir results at perigee from an orbit with 200-km perigee and 1200-km apogee, which approximately equals the ground IFOV for Nimbus-7 TOMS.

Reduced eccentricity results in less Earth coverage loss. Temporary transfer elliptical orbit strategies must have mechanisms on board to reduce extreme eccentricity or suffer Earth coverage loss, and impair the acquisition of long-term ozone data bases.

Finally, an attitude uncertainty of 0.1° on each axis is sufficient, and produces errors < 1.3 DU even under the worst conditions for a 955-km orbit. This error increases with altitude, but only attains a maximum of 1.4 DU at 1200 km.

5.0 REFERENCES

Iqbal, M., 1983: An Introduction to Solar Radiation, Academic Press, New York. 390 pp.

Khan, I. R., 1978: Design and Implementation of Models for Satellite Mission Design Program, JPL EM 312/78-54.

Klenk, K. F., P. K. Bhartia, A. J. Fleig, V. G. Kaveeshwar, R. D. McPeters, and P. M. Smith, 1982: Total Ozone Determination From the Backscattered Ultraviolet (BUV) Experiment, *J. Appl. Meteor.*, **21**, pp. 1672-1684.

Maul, G. A., 1985: Introduction to Satellite Oceanography, Martinus Nijoff Publ. Dordrecht. 606 pp.

Stewart, R. H., 1985: Methods of Satellite Oceanography, Univ. Calif. Press, Berkeley, 360 pp.

Stolarski, R. S., M. R. Schoeberl, P. A. Newman, R. D. McPeters, and A. J. Krueger, 1990: The 1989 Antarctic Ozone Hole as Observed by TOMS, *Geophys. Res. Lett.*, **17**, pp. 1267-1270.

Wertz, J. R., 1978: Spacecraft Attitude Determination and Control, D. Reidel Publ. Co., Boston. 45 pp.

Wilson, W. H., R. C. Smith, and J. W. Nolten, 1981: The CZCS Geolocation Algorithms, SIO Ref. 81-32, Scripps Institution of Oceanography, La Jolla, CA. 37 pp.

NASA
National Aeronautics and Space Administration

Report Documentation Page

1. Report No.	2. Government Accession No.	3. Recipient's Catalog No.
NASA CR-4361		

4. Title and Subtitle

Analysis of Error in TOMS Total Ozone as a Function of Orbit and Attitude Parameters

5. Report Date

April 1991

6. Performing Organization Code

916

7. Author(s)

W. W. Gregg, P. E. Ardanuy, W. C. Braun, B. J. Vallette, P. K. Bhartia, and S. N. Ray

8. Performing Organization Report No.

91B00079

10. Work Unit No.

9. Performing Organization Name and Address

Research and Data Systems Corporation
Greenbelt, MD 20770

11. Contract or Grant No.

NAS5-29373

13. Type of Report and Period Covered

Contractor Report

12. Sponsoring Agency Name and Address

National Aeronautics and Space Administration
Goddard Space Flight Center
Greenbelt, MD 20771

14. Sponsoring Agency Code

15. Supplementary Notes

W. W. Gregg, P. E. Ardanuy, W. C. Braun, and B. J. Vallette: Research and Data Systems Corporation, Greenbelt, MD
P. K. Bhartia: Consultant, Mitchellville, MD
S. N. Ray: Software Corporation of America, Bowie, MD

16. Abstract

Computer simulations of orbital scenarios were performed to examine the effects of orbital altitude, equator crossing time, attitude uncertainty, and orbital eccentricity on ozone observations by future satellites. These effects were assessed by determining changes in solar and viewing geometry and Earth daytime coverage loss. The importance of these changes on ozone retrieval was determined by simulating uncertainties in the TOMS ozone retrieval algorithm. The major findings are as follows: 1) Drift of equator crossing time from local noon would have the largest effect on the quality of ozone derived from TOMS. The most significant effect of this drift is the loss of Earth daytime coverage in the winter hemisphere. The loss in coverage increases from 1° latitude for ± 1 hour from noon, 6° for ± 3 hours from noon, to 53° for ± 6 hours from noon. An additional effect is the increase in ozone retrieval errors due to high solar zenith angles. 2) To maintain contiguous Earth coverage, the maximum scan angle of the sensor must be increased with decreasing orbital altitude. The maximum scan angle required for full coverage at the equator varies from 60° at 600-km altitude to 45° at 1200 km. This produces an increase in spacecraft zenith angle θ, which decreases the ozone retrieval accuracy. The range in θ was $\approx 72°$ for 600 km to $\approx 57°$ at 1200 km. 3) The effect of elliptical orbits is to create gaps in coverage along the subsatellite track. An elliptical orbit with a 200-km perigee and 1200-km apogee produced a maximum Earth coverage gap of about 45 km at the perigee at nadir. 4) An attitude uncertainty of 0.1° in each axis (pitch, roll, yaw) produced a maximum ozone retrieval error of 1.3 Dobson Units at 955 km under the worst conditions (maximum attitude configuration, maximum scan angle to view the pole, and maximum solar zenith angle).

17. Key Words (Suggested by Author(s))	18. Distribution Statement
TOMS, ozone, ozone retrieval algorithm, circular orbits, elliptical orbits, Earth location, ozone profile uncertainty	Unclassified - Unlimited Star Category 47

19. Security Classif. (of this report)	20. Security Classif. (of this page)	21. No. of pages	22. Price
Unclassified	Unclassified	45	A03

NASA FORM 1626 OCT 86